

Evaluation of the Disconnect between Hepatocyte and Microsome Intrinsic Clearance and In Vitro In Vivo Extrapolation Performance[§]

 Beth Williamson, Stephanie Harlfinger, and Dermot F. McGinnity

Drug Metabolism and Pharmacokinetics, Research and Early Development, Oncology R&D, AstraZeneca, Cambridge, United Kingdom

Received May 29, 2020; accepted August 17, 2020

ABSTRACT

The use of *in vitro in vivo* extrapolation (IVIVE) from human hepatocyte (HH) and human liver microsome (HLM) stability assays is a widely accepted predictive methodology for human metabolic clearance (CL_{met}). However, a systematic underprediction of CL_{met} from both matrices appears to be universally apparent, which can be corrected for via an empirical regression offset. After physiological scaling, intrinsic clearance (CL_{int}) for compounds metabolized via the same enzymatic pathway should be equivalent for both matrices. Compounds demonstrating significantly higher HLM CL_{int} relative to HH CL_{int} have been encountered, raising questions regarding how to predict CL_{met} for such compounds. Here, we determined the HLM:HH CL_{int} ratio for 140 marketed drugs/compounds, compared this ratio as a function of physicochemical properties and drug metabolism enzyme dependence, and examined methodologies to predict CL_{met} from both matrices. The majority (78%) of compounds displaying a high HLM:HH CL_{int} ratio were CYP3A substrates. Using HH CL_{int} for CYP3A substrates, the current IVIVE regression offset approach remains an appropriate strategy to predict CL_{met} (% compounds overpredicted/correctly predicted/underpredicted 27/62/11, respectively).

However, using the same approach for HLM significantly overpredicts CL_{met} for CYP3A substrates (% compounds overpredicted/correctly predicted/underpredicted 56/33/11, respectively), highlighting that a different IVIVE offset is required for CYP3A substrates using HLM. This work furthers the understanding of compound properties associated with a disproportionately high HLM:HH CL_{int} ratio and outlines a successful IVIVE approach for such compounds.

SIGNIFICANCE STATEMENT

Oral drug discovery programs typically strive for low clearance compounds to ensure sufficient target engagement. Human liver microsomes and isolated human hepatocytes are used to optimize and predict human hepatic metabolic clearance. After physiological scaling, intrinsic clearance for compounds of the same metabolic pathway should be equivalent between matrices. However, a disconnect in intrinsic clearance is sometimes apparent. The work described attempts to further understand this phenomenon, and by achieving a mechanistic understanding, improvements in clearance predictions may be realized.

Introduction

For oral drug discovery programs, there is typically a requirement to design and develop low clearance (CL) compounds to ensure sufficient extent and duration of target engagement. Optimization of CL is usually one of the more significant challenges in drug discovery. With hepatic metabolic elimination remaining the predominant CL pathway for drugs (Cerny, 2016), the use of *in vitro in vivo* extrapolation (IVIVE) from metabolic stability assays is a widely accepted predictive methodology for human metabolic CL (CL_{met}) (Riley et al., 2005; Bowman and Benet, 2019a,b; Williamson et al., 2020). IVIVE comparisons of measured *in vivo* CL in animal species can assist with developing a cross-species mechanistic understanding of compound disposition.

Moreover, for candidate drugs, successful prediction of an acceptable human *in vivo* CL is important to enable testing of the pharmacological hypothesis in the clinic and thus in reducing drug attrition for pharmacokinetics (PK) reasons (Hay et al., 2014; Davies et al., 2020).

Within drug discovery, two hepatic *in vitro* matrices are primarily used for metabolic stability assays to optimize and predict CL_{met}: human liver microsomes (HLM) and isolated human hepatocytes (HH). HLM offer the ability for enhanced-throughput intrinsic clearance (CL_{int}) screening at relatively low cost and therefore can be used to triage suitable compounds into more expensive hepatocyte incubations. HH are regarded as the most predictive *in vitro* system since they contain the full complement of enzymes and transporters that a compound may encounter during first-pass metabolism, hence they often form the basis of IVIVE for CL_{met}. HLM and HH CL_{int}, corrected for unbound fraction, can be scaled to *in vivo* CL_{int} (ml/min/kg) using physiological parameters (Table 1). Therefore, with the reasonable assumption of

All authors are AstraZeneca employees.

<https://doi.org/10.1124/dmd.120.000131>

[§]This article has supplemental material available at dmd.aspetjournals.org.

ABBREVIATIONS: A-B, apical to basolateral; AAFE, absolute AFE; AFE, average fold error; B-A, basolateral to apical; CL, clearance; CL_{int}, intrinsic CL; CL_{int,u}, scaled unbound CL_{int}; CL_{met}, metabolic CL; ER, efflux ratio; fu_{inc}, fraction unbound in the incubation; HH, human hepatocyte; HLM, human liver microsome; ISEF, intersystem extrapolation factor; IVIVE, *in vitro-in vivo* extrapolation; LC, liquid chromatography; LogD, partition coefficient of a compound between octanol and water at pH7.4; MDCK, Madin-Darby Canine Kidney; MDR, multidrug resistance-1; MS, mass spectrometry; MW, molecular weight; Pgp, P-glycoprotein; PK, pharmacokinetics; Qh, hepatic blood flow; rCYP, recombinant CYP; RED, rapid equilibrium device; RH, rat hepatocyte; UGT, uridine 5'-diphospho-glucuronosyltransferase; V_d, volume of distribution; WSM, "well stirred model".

TABLE 1
Human physiologic scaling factors

Species	Liver Blood Flow (Qh) (ml/min/kg)	Liver Weight (g)	Body Weight (kg)	Microsomal Protein (mg/g Liver)	Hepatocellularity/g Liver
Human	20.7	1500	70	40	120×10^6

similar binding in the HLM and HH incubations and assuming the same metabolic pathways in both systems, the scaled HLM:HH CLint ratio should approximate 1. Indeed, an indicator of the presence of significant additional metabolic pathways, such as glucuronidation, which is present in HH and not HLM (using only NADPH as a cofactor), would be a scaled HLM:HH CLint ratio significantly less than 1.

The commonly accepted approach for IVIVE involves inputting the CLint from HLM and HH into a mathematical model of liver perfusion, typically the “well stirred model” (WSM) (Rowland et al., 1973; Yang et al., 2007), to predict CLmet. However, this approach leads to a systematic underprediction of CLmet for reasons not presently understood (Riley et al., 2005; Foster et al., 2011; Bowman and Benet, 2019a). Many hypotheses to account for this underprediction have been proposed (Bowman and Benet, 2019a; Williamson et al., 2020), all of which should be considered during IVIVE for key compounds. However, none of these explanations solely satisfy the systematic nature of the CLmet underprediction. To account for this underprediction, an empirical correction can be applied to the *in vitro* data from hepatocytes or microsomes. This offset can be derived using a regression approach, in which the derived unbound *in vitro* and *in vivo* CLint values (ml/min/kg) form a correlation line from which future predictions of unbound *in vivo* CLint values for new compounds can be made (Riley et al., 2005; Sohlenius-Sternbeck et al., 2012). Notably, this offset appears to be relatively consistent between liver matrices, species, and laboratories and is independent of compound (Riley et al., 2005; Bowman and Benet, 2016; Wood et al., 2017).

Importantly, for CYP-mediated disposition, which remains the most prevalent CL pathway for drug-like compounds, there appears to be an overall comparable IVIVE predictive performance between HLM and HH (Riley et al., 2005; Chiba et al., 2009; Bowman and Benet, 2016). More recently, it has been postulated that underprediction from both matrices is increased as CL increases (Bowman and Benet, 2019a), and HLM are more accurate for predicting CL of CYP3A substrates (Bowman and Benet, 2019b).

Several reports have also noted a disconnect between HLM and HH CLint (Stringer et al., 2008; Foster et al., 2011; Bowman and Benet, 2019b), whereby a scaled HLM:HH CLint ratio significantly greater than 1 has been determined for specific compounds. Considerably larger CLint values in HLM relative to HH have been observed for CYP3A substrates yet, intriguingly, not for substrates of other drug metabolism enzymes (Bowman and Benet, 2019b). The mechanistic basis for this phenomenon has yet to be elucidated, although it has been hypothesized that this observation could be due to the overlapping substrate specificity between CYP3A and the efflux transporter, P-glycoprotein (Pgp), that is located on the hepatocyte membrane, restricting compound access to drug metabolism enzymes in hepatocytes relative to unhindered access to the same enzymes in microsomes (Bowman and Benet, 2019b), thus resulting in disproportionately lower CLint determined in HH relative to HLM.

Recently, Lombardo et al. (2018) published a large data set of compounds to investigate the relationship between physicochemical properties and human PK. This data set was used to investigate factors contributing to the phenomena, which we have observed in our

laboratory, of the apparent disconnect between HLM and HH CLint and the predictive performance of IVIVE between matrices for such compounds. The data and analyses presented herein provide further insight regarding the HLM:HH CLint disconnect with a significant data set of 140 marketed drugs/compounds. By achieving a mechanistic understanding, improvements in IVIVE accuracy and CL predictions may be realized.

Materials and Methods

Compound Selection. The Lombardo data set (Lombardo et al., 2018) comprised 1352 compounds with measured human PK parameters and physicochemical properties. The data set was cross-referenced with compounds available in the AstraZeneca compound bank and filtered according to the following criteria:

- Compounds with a measured human CL approaching or less than liver blood flow (Qh 20.7 ml/min/kg) were included to disregard compounds with extraordinarily high CL that may have a significant extrahepatic component to their elimination.
- Only compounds with a molecular weight (MW) 150–800 and octanol: water partition coefficient LogD at pH 7.4 (LogD) 0.5–4 were included to broadly represent the typical small-molecule physicochemical property space encountered in oral drug discovery.
- HLM CLint, HH CLint, human plasma protein binding, and incubational binding (fuinc) values were determined. Compounds with limits on measured values (< and >) were subsequently excluded to avoid bias.

The resulting data set ($n = 140$ compounds) mainly comprised biopharmaceuticals class 1 compounds predominantly cleared by hepatic metabolism, with human CL ranging 0.1–20 ml/min/kg. When required, additional data were generated, including Caco-2 permeability (Papp), Caco-2 efflux, Madin-Darby Canine Kidney (MDCK) multidrug resistance mutation 1 (MDR1) efflux, and CYP phenotyping (if the main route of elimination was via CYP, but the contribution of each isoform was unknown from literature sources). Given the reasonable assumption of consistencies in fuinc between species and matrices (Winiwarter et al., 2019), fuinc in HLM or rat hepatocytes (RH) was used. For LogD and fuinc, experimental values were supplemented with the use of *in-house in silico* models generated from machine learning methods. When possible, the main hepatic metabolic route of elimination was obtained from literature references or using databases, including the University of Washington Drug Interaction Database (this information was based on or an extract from Drug Interaction Database Copyright University of Washington, accessed: April 2020) (Supplemental Table 1). It was assumed that the clinical disposition pathway obtained from the literature reflects the main metabolic pathway in HH and HLM. Only in absence of such references were additional *in vitro* reaction phenotyping data obtained to define the main contributing enzyme (Supplemental Table 1).

For all *in vitro* assays detailed below, the experimental work was conducted at the Contract Research Organization, Pharmaron, China.

Materials. HLM (150 donors; Lot QQY and Lot 38289) were purchased from Corning or BioIVT (Shanghai, China), respectively. HH (10 donors; Lot LYB and Lot IRK) were purchased from BioIVT. Human plasma was purchased from BioIVT (mixed donors, with a minimum of two males and two females). Recombinant human CYP enzymes were purchased from CYPLEX (Shanghai, China). EDTA-K2 was purchased from Beijing Chemical Reagents Company (Beijing, China). Bovine serum albumin was purchased from Beijing Xijingke Biotechnology Co., Ltd (Beijing, China). FBS, Hank's balanced salt solution, nonessential amino acids, and the rapid equilibrium device (RED) were purchased from Gibco by Thermo Fisher Scientific (Shanghai, China). Dulbecco's modified Eagle's medium was purchased from Corning. 2-(N-morpholino)ethanesulfonic acid was purchased from Sigma (Shanghai, China). The 96-well equilibrium dialysis plate was purchased from LLC (CT). All other chemicals and materials were purchased from Solarbio S&T Co., LTD (Beijing, China).

Determination of Human Hepatocyte CLint. Test compound was prepared to 10 mM in 100% DMSO and further diluted to 100 μ M in 100% acetonitrile. The hepatocyte incubations were prepared in Leibovitz's L-15 Medium (pH 7.4) containing 1 million hepatocytes/ml and a final compound concentration of 1 μ M. Cell viability was determined using a Cellometer Vision, and >80% cell viability

was required to proceed with the compound incubation. The compound/cell solution (250 μ l) was incubated for 2 hours at 37°C and shaken at 900 rpm on an Eppendorf Thermomixer Comfort plate shaker. Samples (20 μ l) were taken at 0.5, 5, 15, 30, 45, 60, 80, 100, and 120 minutes and quenched with 100 μ l of 100% ice-cold acetonitrile. Samples were shaken at 800 rpm for 2 minutes and centrifuged at 4000 rpm for 20 minutes at 4°C to pellet precipitated protein. The supernatant fraction was diluted 1:5 with deionized water, shaken at 1000 rpm for 2 minutes, and further diluted 1:1 with deionized water. Samples were analyzed by liquid chromatography (LC)–mass spectrometry (MS)/MS.

As described previously (Williamson et al., 2020), submicromolar K_m values (lower than compound assay concentrations) can impact CL_{int}, but occurrence is infrequent, and determination of K_m was beyond the scope of this work. Hence, 1 μ M was selected as an appropriate concentration in the CL_{int} assays.

Determination of Human Microsome CL_{int}. Test compound was prepared to 10 mM in 100% DMSO and further diluted to 100 μ M in 100% acetonitrile. The microsomal incubations were prepared in phosphate buffered solution (pH 7.4) containing 1 mg/ml microsomal protein, 1 mM NADPH, and a final compound concentration of 1 μ M. After a preincubation with NADPH for 8 minutes, reactions were initiated through the addition of the test compound (final volume 250 μ l) and incubated at 37°C in a water bath for 30 minutes. At each time point (0.5, 5, 10, 15, 20, 30 minutes), 20 μ l of incubation mixture was quenched with 100 μ l of 100% ice-cold acetonitrile. Samples were shaken at 800 rpm for 2 minutes and centrifuged at 4000 rpm for 20 minutes at 4°C to pellet precipitated protein. The supernatant fraction was diluted 1:5 with deionized water, shaken at 1000 rpm for 2 minutes, and further diluted 1:1 with deionized water. Samples were analyzed by LC-MS/MS.

Determination of Human Plasma Protein Binding. Plasma protein binding was completed using an RED device. Test compound was prepared to 1 mM in 100% DMSO and further diluted in plasma to achieve a final compound concentration of 5 μ M in the incubation. Immediately, 50 μ l of the spiked plasma was aliquoted as a control T = 0 sample. The T = 0 sample was matrix-matched with 50 μ l of blank phosphate buffered solution (pH 7.4) and quenched with 400 μ l of 100% ice-cold acetonitrile. Phosphate buffered solution (pH 7.4; 500 μ l) was added to the receiver chamber of the RED device, and spiked plasma (300 μ l) was added to the donor chamber. The plate was covered with a gas-permeable lid and incubated for 18 hours at 37°C with 5% CO₂ on an orbital shaker at 300 rpm. Remaining spiked plasma was incubated in a plastic plate for 18 hours at 37°C with 5% CO₂ on an orbital shaker at 300 rpm, representing an T = 18 hours sample. At the end of incubation, 50 μ l of post dialysis sample from the donor or T = 18 sample and receiver wells were aliquoted into separate wells and matrix matched with 50 μ l of phosphate buffered solution (pH 7.4) or blank plasma, respectively. The samples were subsequently quenched separately in 400 μ l of ice-cold 100% acetonitrile. Quenched samples, including T = 0, were shaken at 1000 rpm for 10 minutes and centrifuged for 30 minutes at 4000 rpm to pellet precipitated protein. The supernatant fraction was further diluted 1:1 with deionized water for analysis by LC-MS/MS. An eight-point calibration curve (1–7500 nM) matrix matched with plasma or phosphate buffered solution and quenched with 400 μ l of ice-cold 100% acetonitrile was used to determine the concentration in the donor and receiver wells. Compound recovery and stability in the plasma were determined using the T = 0 and T = 18 samples.

Determination of fu_{inc}. HLM or RH binding was completed using a 96-well equilibrium dialysis plate. Test compound was prepared to 100 μ M in 100% DMSO and further diluted in 1 mg/ml HLM/phosphate buffer or 1 X 10⁶ inactivated (1 hour incubation with 1 mM 1-Aminobenzotriazole and 1.5 mM salicylamide) RH/phosphate buffer to achieve a final compound concentration of 1 μ M in the incubation. Immediately, 50 μ l of the spiked RH or HLM/phosphate buffered solution was aliquoted as a control T = 0 sample. The T = 0 sample was matrix matched with 50 μ l of blank phosphate buffered solution (pH 7.4) and quenched with 400 μ l of 100% ice-cold acetonitrile. Phosphate buffered solution (pH 7.4; 150 μ l) was added to the receiver chamber of the dialysis block and spiked HLM/RH suspension (150 μ l) was added to the donor chamber. The plate was covered with a gas-permeable lid and incubated for 4 hours at 37°C with 5% CO₂ on an orbital shaker at 350 rpm. Remaining spiked matrix was incubated in a plastic plate for 18 hours at 37°C with 5% CO₂ on an orbital shaker at 300 rpm, representing an T = 18 hours sample. At the end of incubation, 50 μ l of postdialysis sample from the donor or T = 18 sample and receiver wells were matrix-matched with 50 μ l of phosphate buffered solution (pH 7.4) or blank RH or HLM/phosphate buffer, respectively. The samples were subsequently

quenched separately in 400 μ l of ice-cold 100% acetonitrile. Quenched samples were shaken at 1000 rpm for 10 minutes and centrifuged for 30 minutes at 4000 rpm to pellet precipitated protein. The supernatant fraction was further diluted 1:1 with deionized water for analysis by LC-MS/MS. For RH fu_{inc}, a five-point calibration curve (1–2000 nM) was generated, and for HLM fu_{inc}, a six-point calibration curve (1–2000 nM) was generated. Each standard was matrix matched with RH or HLM/phosphate buffer and phosphate buffered solution and quenched with 400 μ l of ice-cold 100% acetonitrile. The calibration curve was used to determine the concentration in the donor and receiver wells. Compound recovery and stability in the matrix were determined using the T = 0 and T = 18 samples.

Determination of Caco-2 or MDCK-MDR1 Permeability and Cell Efflux Ratio. Test compound was prepared to 10 mM in 100% DMSO and further diluted to 200 μ M in 100% acetonitrile. Caco-2 and MDCK-MDR1 cells were diluted in Dulbecco's modified Eagle's medium (culture medium) at a density of 6.86 X 10⁵ and 1.56 X 10⁶ cells/ml, respectively. Fifty microliters of cell suspension was added to a 96-well transwell insert plate containing 50 μ l of culture medium. The base plate contained 25 ml of culture medium. The Caco-2 cells were cultured for 14–18 days, and MDCK cells were cultured for 4–8 days, with culture medium replaced every other day. Once confluent (as determined by lucifer yellow) and electrical resistance was >230 Ω .cm² for Caco-2 or >42 Ω .cm² for MDCK, the cells were used in the assay. The cells were washed and incubated with Hank's balanced salt solution containing 25 mM HEPES (pH 7.4) (transport buffer) for 30 minutes. Compounds were diluted to 2 mM in 100% DMSO and then further diluted to 10 μ M in transport buffer. To determine the rate of compound transport in the apical to basolateral (A-B) direction, 108 μ l of the 10 μ M compound solution was added to the transwell (apical), and 300 μ l of transport buffer was added to the receiver well (basolateral). Immediately, 8 μ l from the apical compound solution was diluted in 72 μ l of transport buffer and quenched with 240 μ l of ice-cold 100% acetonitrile; this sample represented a control T = 0 sample. Similarly, to determine the rate of compound transport in the basolateral to apical (B-A) direction, 308 μ l of the 10 μ M compound solution was added to the receiver well (basolateral), and 100 μ l of transport buffer was added to the transwell (apical). A T = 0 sample was immediately prepared by diluting 8 μ l from the basolateral compound solution in 72 μ l of transport buffer and quenching with 240 μ l of ice-cold 100% acetonitrile. The plates were then incubated at 37°C for 2 hours. At the end of the 2 hour incubation, 8 μ l of sample was aliquot from the donor side (apical for A-B and basolateral for B-A) and added to 72 μ l of transport buffer and 240 μ l of ice-cold 100% acetonitrile. For the receiver compartments (basolateral for A-B and apical for B-A), 72 μ l was aliquoted and added to 240 μ l of ice-cold 100% acetonitrile. Quenched samples were shaken at 1000 rpm for 5 minutes and centrifuged for 20 minutes at 4000 rpm to pellet precipitated protein. The supernatant fraction was further diluted 1:1 with deionized water for analysis by LC-MS/MS.

CYP Reaction Phenotyping. Test compound was prepared to 10 mM in 100% DMSO and further diluted to 200 μ M in 100% acetonitrile. Recombinant human CYP (rCYP: CYP3A4, CYP3A5, CYP2C9, CYP2C19, CYP2C8, CYP1A2, CYP2D6, CYP2E1, CYP2B6) were diluted with phosphate buffered solution (pH 7.4) to achieve a final concentration of 112 pmol/ml. The diluted CYP solution was preincubated with test compound (final concentration 2 μ M) at 37°C for 15 minutes. The reaction was initiated through the addition of the 10 mM NADPH and incubated at 37°C on a plate shaker at 100 rpm for 30 minutes. At each time point (2.5, 5, 10, 15, 20, 30 minutes), 30 μ l of incubation mixture was quenched with 120 μ l of 100% ice-cold acetonitrile. Samples were shaken at 1000 rpm for 10 minutes and centrifuged at 4000 rpm for 20 minutes. The quench plate was further incubated at 4°C for 30 minutes and recentrifuged at 4000 rpm for 20 minutes to pellet precipitated protein. The supernatant fraction was diluted 1:1 with deionized water, shaken at 1000 rpm for 2 minutes, and analyzed by LC-MS/MS.

LC-MS/MS Analysis. The MS/MS instrument used was either a Waters XEVO TQ-S, Waters XEVO TQ-D, or API 4000 (AB Sciex). The ultra-mass spectrometer used for sample analysis was completed in the multiple reaction monitoring mode (MS/MS). Reverse-phase high performance liquid chromatography with a C18 column was used to separate the analytes. A mobile phase of 99% water/0.1% formic acid (solvent A) and a solvent phase of 99% acetonitrile/0.1% formic acid (solvent B) was used. A generic LC gradient elution was used at a flow rate of 0.5 ml/min with 95% solvent A and 5% solvent B for 0.3 minutes, after which the concentration of solvent B was increased to 95% over 0.9 minutes

before restoring it back to 5% for the remaining 0.5 minutes. Mass-spectrometer methods were optimized for each compound.

For all assays, the 100% ice-cold acetonitrile used to quench the samples contained internal standards to ensure efficient extraction of sample, confirm injection into the mass spectrometer, and allow assessment of ionization variability. Data were accepted if the internal standard peak area coefficient of variation was <20%.

Data Analysis. The $t_{1/2}$ and, subsequently, the CLint of the compounds incubated in HH or HLM were calculated according to eqs. 1 and 2.

$$t_{1/2}(\text{min}) = \frac{\text{Ln}(2)}{-\text{slope}}. \quad (1)$$

$$CL_{\text{int}}(\mu\text{L}/\text{min} / \times 10^6 \text{ cells or mg protein}) = \frac{\text{Ln}(2) \times V}{t_{1/2}}. \quad (2)$$

In which V ($\mu\text{L}/\times 10^6$ cells or mg protein) is the incubation volume (μL) divided by the number of cells ($\times 10^6$) or microsomal protein content (mg) in the incubation.

The unbound fraction (fu) of the compounds in human plasma, HLM, or RH was calculated according to eq. 3:

$$\text{Fraction unbound (fu)} = \frac{[\text{Compound}]_{\text{Receiver}}}{[\text{Compound}]_{\text{Donor}}}. \quad (3)$$

Compound recovery and stability in the relevant matrix were determined according to eqs. 4 and 5:

$$\text{Compound recovery (\%)} = \frac{[\text{Compound}]_{\text{Receiver}} + [\text{Compound}]_{\text{Donor}}}{[\text{Compound}]_{T=0}} \times 100. \quad (4)$$

$$\text{Compound remaining at 18 h (\%)} = \frac{[\text{Compound}]_{T=18}}{[\text{Compound}]_{T=0}} \times 100. \quad (5)$$

The $t_{1/2}$ and, subsequently, the CLint of the compounds incubated with rCYP were determined as detailed in eqs. 6 and 7:

$$t_{1/2, \text{rCYP}}(\text{min}) = \frac{\text{Ln}(2)}{-\text{slope}}. \quad (6)$$

$$CL_{\text{int, rCYP}}(\mu\text{L}/\text{min}/\text{pmol}) = \frac{\text{Ln}(2) \times V}{t_{1/2}}. \quad (7)$$

In which, V ($\mu\text{L}/\text{mg}$ protein) is the incubation volume divided by the mg of protein in the incubation.

The $CL_{\text{int, rCYP}}$ was further scaled to account for CYP450 abundance and the intersystem extrapolation factors (ISEFs) utilizing the respective values incorporated in Simcyp (v19) using eq. 8:

$$CL_{\text{int, CYP}_i}(\mu\text{L}/\text{min}/\text{mg protein}) = CL_{\text{int, rCYP}_i} \times \text{CYP}_i \text{ abundance} \times \text{ISEF}_{\text{CYP}_i}. \quad (8)$$

In which CYP_i is the i th CYP isoform tested out of n CYP isoforms. $CL_{\text{int, CYP}_i}$ is the scaled CLint for the i th CYP isoform, $CL_{\text{int, rCYP}_i}$ is the CLint determined for the i th CYP isoform in rCYP ($\mu\text{L}/\text{min}/\text{pmol}$) (eq. 7), CYP_i abundance is the abundance of the i th CYP isoform in the HLM (pmol of cytochrome P450/mg protein), and $\text{ISEF}_{\text{CYP}_i}$ is the ISEF for the i th CYP isoform.

The scaled $CL_{\text{int, CYP}}$ values were summed to give the total scaled CLint in HLM, and the contribution of each CYP isoform in HLM was determined according to eq. 9.

$$\text{Contribution}_{\text{CYP}_i}(\%) = \frac{CL_{\text{int, CYP}_i}}{\sum_{i=1}^n CL_{\text{int, CYP}_i}} \times 100. \quad (9)$$

HLM:HH CLint ratio. Scaled HH and scaled HLM CLint values (ml/min/kg, eq. 10) were compared for each compound to calculate the difference, which was referred to as HLM:HH CLint ratio. Specifically, scaled HLM CLint (ml/min/kg) was divided by scaled HH CLint (ml/min/kg). Assuming incubational binding was consistent between HLM and HH (Chen et al., 2017; Winiwarter et al., 2019), the difference in scaled CLint (ml/min/kg) between the matrices was expected to be ~ 1 (based on the physiologic scaling factors noted in Table 1).

HLM or HH scaled CLint (mL/min/kg)

$$= \left[(\text{microsomal protein (mg/g liver)} \text{ OR } \text{hepatocellularity} (\times 10^6/\text{g liver})) \times \frac{\text{liver weight (g)}}{\text{body weight (kg)}} \right] / 1000. \quad (10)$$

IVIVE. To compare *in vitro* hepatic CLint and *in vivo* CL for the 140 compound set, the WSM (eq. 11) (Rowland et al., 1973; Yang et al., 2007) was applied with a regression offset to correct for the observed systematic underprediction of *in vivo* CL:

$$CL_{\text{met}}(\text{ml}/\text{min}/\text{kg}) = \frac{(Q_h \times fu \times CL_{\text{int, u}})}{(Q_h + fu \times CL_{\text{int, u}})}. \quad (11)$$

Where, CL_{met} is the *in vivo* CL determined in plasma (assuming CL is hepatic metabolic), Q_h is hepatic blood flow (ml/min/kg), fu is the free fraction determined in plasma, and $CL_{\text{int, u}}$ is the scaled unbound intrinsic metabolic CL determined from HH or HLM (ml/min/kg).

Regression Offset Approach.

1. HH or HLM CLint values corrected for fuinc were scaled to the whole liver using physiological scaling factors (eq. 10; Table 1) to generate an *in vitro* CLint,u (units: ml/min/kg).
2. *In vivo* CLint (units: ml/min/kg) was back-calculated from human *in vivo* CLtotal values (*in vivo* CLint,u ml/min/kg), assuming hepatic metabolic CL and using the WSM (eq. 11) to deconvolute hepatic blood flow and fu in the blood (Yang et al., 2007).
3. Using a training set of 24 metabolically cleared drugs, the *in vitro* CLint,u and *in vivo* CLint,u values were compared for HH and HLM. A systematic underprediction of *in vivo* CLint,u from *in vitro* CLint,u was observed for both matrices. In our laboratory, the regression offset required to correct the underprediction was 3-fold for HLM and HH (Riley et al., 2005; Sohlenius-Sternbeck et al., 2012).
4. For the 140 compound set, the regression offset, previously defined as 3-fold (see point 3 above), was applied prospectively to the *in vitro* CLint,u from HH and HLM and compared with the *in vivo* CLint,u values. If the CLint,u values (regression offset applied) for a compound were within 3-fold of unity, CLmet was categorized as correctly predicted. Overpredictions and underpredictions of *in vivo* CLint,u were categorized as greater than 3-fold differences.
5. For scaling without the application of a regression offset, the *in vitro* CLint,u was calculated solely using the WSM (eq. 11).

Caco-2 and MDCK-MDR1 Papp (eq. 12) and, subsequently, efflux ratio were determined according to eq. 13:

$$P_{\text{app}}(\times 10^{-6} \text{ cm/s}) = \frac{V_A}{\text{Area} \times \text{Time}} \times \frac{[\text{Compound}]_{\text{Acceptor}}}{[\text{Compound}]_{\text{Initial donor}}}. \quad (12)$$

In which, V_A is the volume in the acceptor well, Area is the surface area of the membrane, and Time is the total transport time.

$$\text{Efflux ratio} = \frac{P_{\text{app}}(B-A)}{P_{\text{app}}(A-B)}. \quad (13)$$

The average fold error (AFE) (eq. 14) and absolute average fold error (AAFE) (eq. 15) were calculated to determine the bias (AFE) and precision (AAFE) of the CL predictions:

$$AFE = 10^{\frac{1}{n} \sum \log \left(\frac{\text{Observed}}{\text{Predicted}} \right)}. \quad (14)$$

$$AAFE = 10^{\frac{1}{n} \sum \left| \log \left(\frac{\text{Observed}}{\text{Predicted}} \right) \right|}. \quad (15)$$

HLM:HH CLint ratio data were not normally distributed. Therefore, a Kruskal-Wallis with Dunn's multiple comparison correction was used to determine whether there was a difference in HLM:HH CLint ratio median between compounds for different classes (e.g., ion class, main metabolizing enzymes, etc.). To determine the Kruskal-Wallis statistic (H) and the probability (P), all data were pooled (ignoring the group from which the data belong) and ranked in ascending order. The rank sums were then combined to generate the P value and

a single statistic value termed *H*. A large *H* refers to a large difference between rank sums. If the Kruskal-Wallis test was significant, a Dunn's multiple comparison was used to determine which groups were statistically different from each other by calculating a *P* value (McDonald, 2014a; Dinno, 2015; Weaver et al., 2017).

A paired *T* test was used to compare HLM and HH CL_{int,u} for uridine 5'-diphospho-glucuronosyltransferase (UGT), CYP1A, CYP2C, CYP2D6, and others because the variables were normally distributed, and a Wilcoxon matched-pairs signed rank test (McDonald, 2014b) was used to compare HLM and HH CL_{int,u} for CYP3A because the variable was not normally distributed.

Results

HLM:HH CL_{int} Ratio Dependencies. Assuming similar metabolic rates and routes, scaled HLM and HH CL_{int} (*in vitro* CL_{int,u} ml/min/kg) were expected to be equivalent (HLM:HH CL_{int} ratio = 1). In our data set, 51% of compounds had an HLM:HH CL_{int} ratio ~1, with a maximum observed HLM:HH CL_{int} ratio of 15. The mean HLM:HH CL_{int} ratio was 1.9, and the median was 1.1 for the 140 compound data set. Inherent experimental variability in the HLM and HH *in vitro* assays was assessed (unpublished data), and ~95% of replicate CL_{int} determinations for the same compound were within 2-fold. Thus, we categorized HLM:HH CL_{int} ratio ≥2-fold as a significant biologic difference.

The HLM:HH CL_{int} ratio was significantly different between bases (mean 2.1) and acids (mean 1.0). However, the HLM:HH CL_{int} ratio was not significantly different between neutrals and acids or neutrals and bases (Fig. 1A). HLM:HH CL_{int} ratio was not correlated with MW, LogD, pKa, human Vd, or human CL (Fig. 1, B–F).

The dependence between the main metabolizing enzyme for compounds and HLM:HH CL_{int} ratio was evaluated for the compound data set. The HLM:HH CL_{int} ratio varied between metabolizing enzymes with the highest HLM:HH CL_{int} ratio observed for CYP3A substrates (mean/median HLM:HH CL_{int} ratio = 2.8/2.1) (Fig. 2; Supplemental Table 1). The difference in *in vitro* scaled CL_{int} between HH and HLM was significantly different for CYP3A substrates (Wilcoxon matched pairs: *P* < 0.0001). UGT substrates displayed a mean HLM:HH CL_{int} ratio >1, but the median was 0.8. For CYP2C, CYP2D6, and CYP1A substrates, the HLM:HH CL_{int} ratio was ~1 (Fig. 2). The data set also contained 16 compounds (11%, referred to as “Other” in Fig. 2) that were reported to be cleared via enzymes other than the major CYPs or UGTs, or the route was not defined, and the mean HLM:HH CL_{int} ratio was 1.4. Interestingly, the vast majority (78%) of compounds with an HLM:HH CL_{int} ratio ≥2 were CYP3A substrates. CYP3A HLM:HH CL_{int} ratio was significantly different to the ratio determined for CYP2C, CYP2D6, and “other” substrates.

Overlapping substrate specificities between CYP3A and Pgp were investigated to understand whether efflux in HH provided an explanation for the high HLM:HH CL_{int} ratio (Fig. 3). Caco-2 efflux ratio (ER) and MDCK-MDR1 ER were determined for 41 and 28 compounds, respectively, and represent compounds from all metabolizing enzyme families. For compounds with an ER >2 in Caco-2 and MDCK-MDR1 cells, the mean/median HLM:HH CL_{int} ratio was 3.8/3.1 and 2.7/2.5, respectively. This was in contrast to the compounds with an ER <2, which displayed mean/median HLM:HH CL_{int} ratio of 1.3/1.0 and 1.6/1.1 in Caco-2 and MDCK-MDR1 cells, respectively. For compounds with an HLM:HH CL_{int} ratio ≥2, 50% and 64% of these compounds displayed an ER >2 in Caco-2 and MDCK-MDR1, respectively. For CYP3A substrates that had an HLM:HH CL_{int} ratio ≥2, 55% had an ER >2 in Caco-2 cells, and 67% had an ER >2 in MDCK-MDR1 cells.

In Vitro In Vivo Extrapolation. IVIVE accuracy of *in vivo* CL_{int,u} was evaluated using both the regression offset approach and with no offset applied for HLM and HH as outlined in *Materials and Methods*.

When evaluating the set of 140 compounds as a whole, IVIVE performance using the regression offset showed minimal bias and good precision for both matrices. For HH, AFE was 1.3, AAFE was 2.9, and % compounds overpredicted/correctly predicted/underpredicted was 25/62/13, respectively, whereas for HLM, AFE was 1.6, AAFE 3.6, and % compounds overpredicted/correctly predicted/underpredicted was 34/52/14, respectively.

Prediction accuracy using the regression offset was comparable between HLM and HH when evaluating subcategories of UGT, CYP2D6, CYP2C, CYP1A, and “other” substrates (Figs. 4 and 5). However, using HLM and the regression offset approach for CYP3A substrates demonstrated a clear overprediction bias (AFE 3.1, AAFE 4.8, % compounds overpredicted/correctly predicted/underpredicted 56/33/11, respectively) (Fig. 4E; Table 2). A comparison between CYP3A and non-CYP3A substrates using HLM and the regression offset approach is shown in Fig. 6. Conducting IVIVE using HLM without a regression offset for CYP3A substrates broadly corrected this overprediction bias (AFE 1.0, AAFE 3.2, % compounds overpredicted/correctly predicted/underpredicted 20/61/19, respectively, Fig. 6B; Table 2). However, using this approach (HLM without a regression offset) for the remaining non-CYP3A substrates led to a marked underprediction of *in vivo* CL_{int,u} (AFE 0.3, AAFE 4.4, % compounds overpredicted/correctly predicted/underpredicted 4/34/62, respectively, Fig. 6B; Table 2).

Using HH and the regression offset for CYP3A substrates demonstrated no clear bias (AFE 1.6, AAFE 3.1, % compounds overpredicted/correctly predicted/underpredicted 27/62/11, respectively) (Fig. 5E; Table 2). Likewise, a comparison between CYP3A and non-CYP3A substrates using HH showed no discernible difference in predictive performance (Fig. 6C; Table 2). It followed that conducting IVIVE using HH without a regression offset resulted in a significant underprediction bias for both CYP3A and non-CYP3A compounds (Table 2).

Discussion

To ensure sufficient target engagement, CL is often a key parameter to optimize before progression of oral candidate drugs into clinical development. With the majority of drugs eliminated via hepatic metabolic enzymes (Cerny, 2016), low CL_{int} in HLM and HH is targeted, and the values are used to predict human metabolic CL. A systematic underprediction of *in vivo* CL_{int} from both these hepatic matrices appears to be universally apparent (Riley et al., 2005; Sohlenius-Sternbeck et al., 2012; Bowman and Benet, 2019a), although it can be corrected for via a regression offset approach (Riley et al., 2005; Sohlenius-Sternbeck et al., 2012) and has been used prospectively to allow successful prediction of *in vivo* CL for many candidate drugs in our laboratory (Davies et al., 2020).

Typically, both HLM and HH are used in drug discovery. Once scaled, the HLM:HH CL_{int} ratio should be ~1 for drugs cleared by the same drug metabolism enzyme pathways in both systems. However, significant differences between HLM and HH CL_{int} have been highlighted by several groups (Stringer et al., 2008; Foster et al., 2011; Bowman and Benet, 2019b), and this “HLM:HH disconnect” has also been observed in our laboratory. When encountered in drug discovery, this HLM:HH disconnect phenomenon poses challenges; firstly to understand the reason(s) for differences in CL_{int} for compounds cleared by the same enzymes and secondly to decide how to approach IVIVE for compounds that demonstrate this disconnect.

No correlation was observed between HLM:HH CL_{int} ratio and human *in vivo* CL, human Vd, LogD, MW, or compound pKa for the 140 compound dataset (Fig. 1). The lack of correlation between HLM:HH CL_{int} ratio and pKa is consistent with the hypothesis that the pH

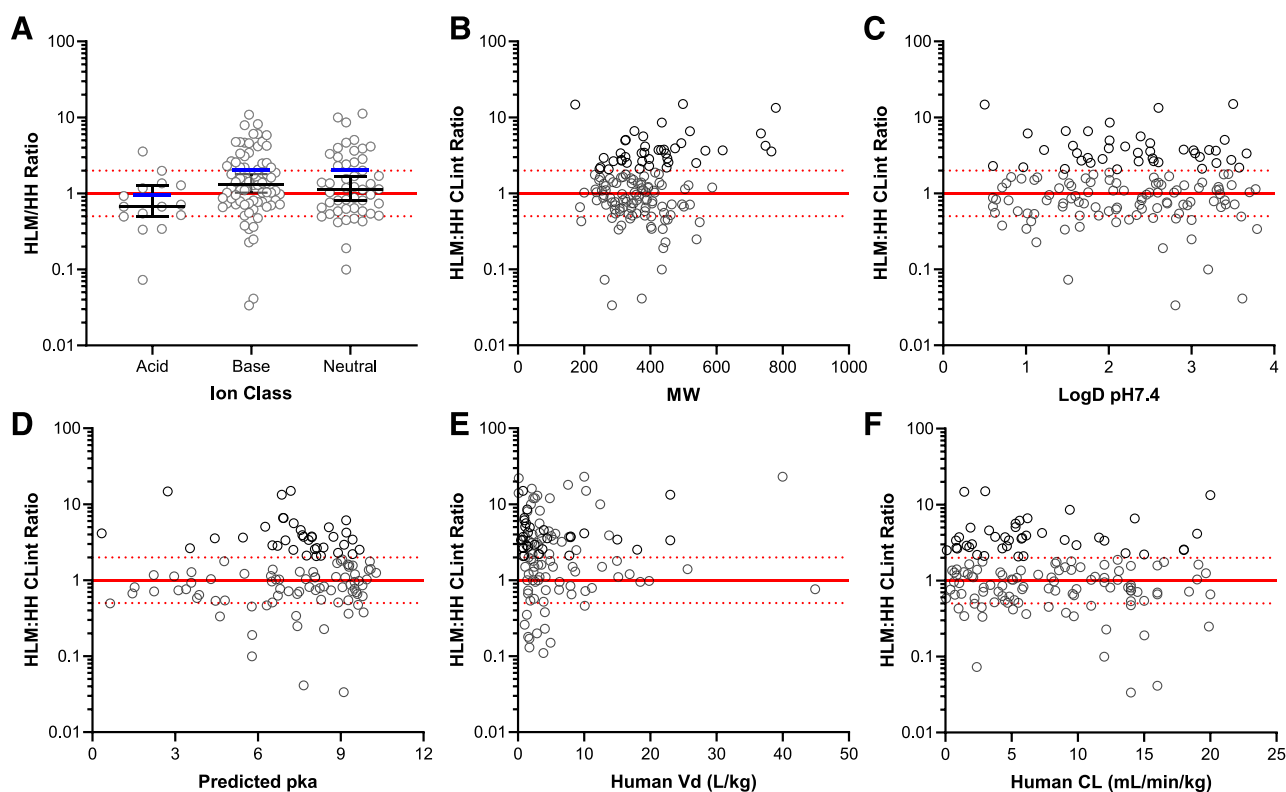
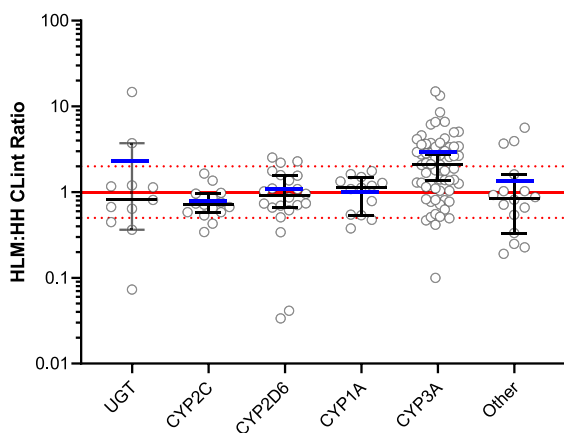


Fig. 1. Relationship between HLM:HH CLint ratio and physicochemical properties or human PK: (A) Ion class, (B) MW, (C) LogD, (D) Predicted pKa, (E) Human Vd and (F) Human CL. Where, in (A) the black box and whisker represent the median and 95% confidence intervals, and the blue solid line is the mean and in (A-F) the solid red horizontal line represents no difference in scaled HLM and HH CLint, and the dashed red horizontal lines represent a 2-fold difference in scaled HLM and HH CLint. HLM:HH CLint ratio was significantly different between bases (mean 2.1) and acids (mean 1.0) (Kruskal-Wallis: $P < 0.0001$, $H = 53.9$, Dunn's: acids-bases $P = 0.036$). The HLM:HH CLint ratio was not significantly different between acids and neutrals or neutrals and bases.

integrity of hepatocytes in suspension is destroyed (Berezhkovskiy, 2011), resulting in the same levels of ionized species present in hepatocyte and microsome assays conducted at pH 7.4. However, there was an observation that neutrals and bases (HLM:HH CLint ratio 2.1) demonstrate this HLM:HH disconnect more so than acids (HLM:HH CLint ratio 1.0), but this difference was only significant between acids and bases and would need more data specifically using acids to confirm. Another consideration is the potential for acids to be substrates of the hepatic organic anion transporting polypeptides (OATPs) present on the membrane of HH. Active uptake into HH has the potential to become the rate-limiting step for the CL of these compounds. However, as shown previously (Di et al., 2012) and as further exemplified here, there was no difference in HLM:HH CLint ratio between OATP substrates [including paritaprevir, lesinurad, and repaglinide (Shebley et al., 2017; <https://didb.druginteractionsolutions.org/drug/monograph/11166/#main-transporters>; <https://didb.druginteractionsolutions.org/drug/monograph/1269/#main-transporters>)] and non-OATP substrates, suggesting there is no OATP dependence for the HLM:HH CLint ratio.

Building on the work by Bowman and Benet (2019b), the association of HLM:HH CLint ratio and metabolism via the major hepatic metabolic enzymes was assessed (Fig. 2). For CYP1A, CYP2C, and CYP2D6 substrates, the HLM:HH CLint ratio value was ~ 1 , consistent with the CLint routes and rates being similar between matrices. Although UGT substrates displayed a high mean HLM:HH CLint ratio, this was influenced by two outliers (edaravone and mizolastine). The median HLM:HH CLint ratio was 0.8, < 1 , as would be expected with the additional metabolism routes present in HH versus HLM. In agreement with Bowman and Benet (2019b), CYP3A substrates displayed a significantly higher CLint in HLM versus HH. These data conducted

on such a large number of compounds confirm that this HLM:HH disconnect phenomenon is highly, if not exclusively, associated by cause or effect with CYP3A substrates. This would also explain the emerging trend that acids, which are not typically substrates of CYP3A, tend not to demonstrate this phenomenon. A thorough mechanistic understanding of the basis for the high HLM CLint relative to HH CLint and the explanation for the strong association of this phenomenon toward CYP3A substrates are clearly desirable. Efflux transporter activity in hepatocytes has been hypothesized to restrict compound access to metabolism enzymes in hepatocytes relative to unhindered access to the same enzymes in microsomes, thus leading to a high liver microsome: hepatocyte CLint ratio (Huang et al., 2010). Hence, overlapping substrate specificities between CYP3A and Pgp (Kim et al., 1999) may contribute to the observed HLM:HH CLint disconnect (Bowman and Benet, 2019b). We considered the relationship between ER and HLM:HH CLint ratio and determined that efflux transporter substrates displayed an HLM:HH disconnect (HLM:HH CLint ratio > 2), whereas non-efflux substrates demonstrated an average HLM:HH CLint ratio of ~ 1 , the theoretical expected ratio, irrespective of the cell line used to determine efflux potential (Fig. 3). These data suggest that an HLM:HH disconnect may be apparent for efflux substrates as a result of Pgp activity restricting CLint in HH relative to HLM. However, only $\sim 50\%$ of CYP3A substrates that displayed an HLM:HH CLint ratio ≥ 2 had an ER > 2 , as determined in either MDCK or Caco-2 cells. Therefore, it would appear that the reason CYP3A substrates demonstrate this phenomenon as a class is not exclusively explained by Pgp activity. Additional confirmatory work would be beneficial to explore the dependence on HLM:HH CLint ratio with Pgp and other transporter activity. It should be noted that all efflux substrates in this



	UGT	CYP2C	CYP2D6	CYP1A	CYP3A	Other
No. of compounds	11	15	22	13	63	16
Mean	2.3	0.8	1.1	1	2.8	1.4
Median	0.8	0.7	0.9	1.1	2.1	0.9
Median 95% CI	0.4 - 3.7	0.6 - 1.0	0.7 - 1.6	0.5 - 1.5	1.4 - 2.8	0.3 - 1.6

Fig. 2. Evaluation of HLM:HH CLint ratio and the main metabolizing enzyme. Where, the black box and whisker solid lines represent the median and 95% confidence intervals (CI), and the blue solid line is the mean. The solid red horizontal line represents no difference in scaled HLM and HH CLint, and the dashed red horizontal lines represent a 2-fold difference in scaled HLM and HH CLint. CYP3A HLM:HH CLint ratio was significantly different to CYP2C, CYP2D6, and Other (Kruskal-Wallis $P < 0.0001$, $H = 29.4$, Dunn's: $P = 0.0006$, $P = 0.009$, and $P = 0.03$, respectively).

data set (when measured) were highly permeable in the Caco-2 assay, suggesting passive permeability across a cell membrane was not a rate-limiting factor in hepatocytes. Furthermore, no correlation was observed between HLM:HH CLint ratio and passive permeability (unpublished data). There may be further additional contributory factors other than transporter activity that may lead to high HLM:HH CLint ratio, for example, whether the high HLM:HH CLint for CYP3A substrates is associated with cryopreserved and not freshly prepared HH. Hepatocyte cryopreservation would have to specifically decrease CYP3A isoform activity, possibly because of conformational changes in the enzyme or via affecting cofactor levels. Considering the high proportion of candidate drugs that are CYP3A substrates, more work in our laboratory and others is warranted.

Although the use of a regression offset approach to correct the widely reported systematic underprediction of *in vivo* CLint is a pragmatic solution to predict CL, it is not mechanistically satisfactory given the empirical nature of this approach. Similar to previous reports, from our

laboratory and others (Riley et al., 2005; Sohlenius-Sternbeck et al., 2012), IVIVE predictive capability utilizing the regression offset approach for the whole dataset of compounds was broadly similar between HH and HLM; 62% and 52% of compounds predicted *in vivo* CLint,u within 3-fold from HH (AFE 1.3, AAFE 2.9) and HLM (AFE 1.6, AAFE 3.6).

Approximately 80% of compounds in this data set with an HLM:HH CLint ratio ≥ 2 were CYP3A substrates, and likewise, our in-house experience with propriety AstraZeneca compounds demonstrates this phenomenon being strongly associated with CYP3A substrates. Given this strong association and the preponderance of candidate drugs metabolized primarily by CYP3A, our analysis focused on comparing and contrasting IVIVE performance for CYP3A versus non-CYP3A substrates. It was observed that when using HLM with an IVIVE regression offset approach for CYP3A substrates (Figs. 4E and 6A; Table 2), there was an overprediction (>3 -fold) of *in vivo* CLint,u (AFE 3.1) for 56% compounds, with only 33% correctly predicted. Not using the regression offset corrected this overprediction so that AFE approached 1, and the number of CYP3A substrates overpredicted reduced from 56% to 20%, and those correctly predicted increased from 33% to 61% (Fig. 6B; Table 2). These data are consistent with previous reports for CYP3A substrates, which employed IVIVE without the use of a regression offset and demonstrated good IVIVE accuracy from HLM (Bowman and Benet, 2019b). However, using HLM without a regression offset for non-CYP3A substrates led to a marked underprediction of *in vivo* CLint,u (AFE 0.3) for 62% compounds, with 34% correctly predicted (Fig. 6B; Table 2). These data highlight that when using HLM for IVIVE, a different regression offset factor is optimal for scaling CYP3A substrates versus non-CYP3A substrates. A full mechanistic understanding is not immediately apparent, but the observation of both CYP isoform and matrix dependence on IVIVE methodology to predict CLmet may help to delineate the underlying reasons in the future. Based on these analyses, it is important to carefully consider IVIVE approaches so that CL is appropriately predicted from HLM data for each substrate class (Riley et al., 2005; Chiba et al., 2009; Bowman and Benet, 2016).

In contrast, for HH, no prediction bias using the IVIVE regression offset approach existed for all categories of compound, including CYP3A substrates, with 62% of such compounds correctly predicted (AFE 1.6, AAFE 3.1) (Fig. 6C; Table 2). Overall, using HH, IVIVE performance using the regression offset approach for the whole data set showed minimal bias and good precision (AFE 1.3, AAFE 2.8) and correctly predicted CLint,u within 3-fold for 62% of compounds, a comparable performance to CYP3A substrates.

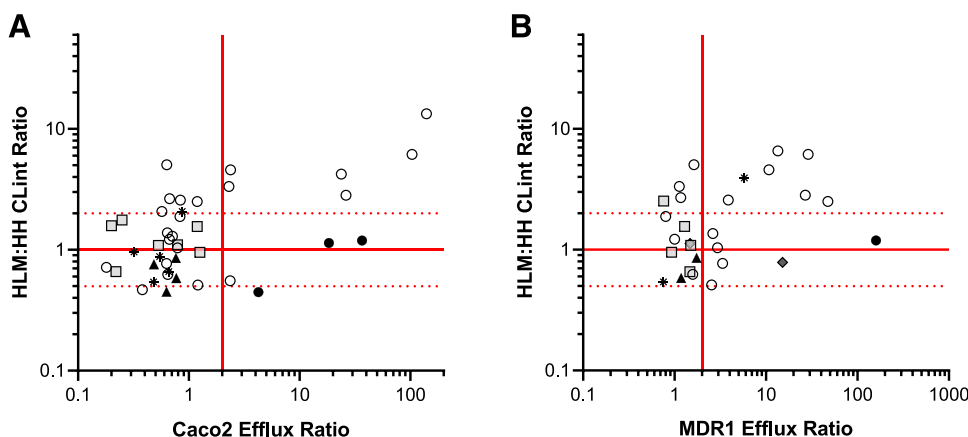


Fig. 3. HLM:HH CLint ratio compared with ER determined in (A) Caco-2 cells and (B) MDCK-MDR1 cells. Where, the solid red horizontal line represents no difference in scaled HLM and HH CLint, the dashed red horizontal lines represent a 2-fold difference in scaled HLM and HH CLint, and the solid red vertical line represents the efflux transporter substrate categorization; ≥ 2 = efflux substrate, < 2 = not an efflux substrate. Symbols represent the main metabolizing enzyme: ●, UGT; ○, CYP3A; ■, CYP2D6; ▲, CYP2C; ◆, CYP1A; and *, Other. In Caco-2, the number of compounds from each metabolizing enzyme group was: UGT $n = 3$, CYP3A $n = 22$, CYP2D6 $n = 7$, CYP2C $n = 4$, CYP1A $n = 0$, and Other $n = 5$. In MDCK-MDR1, UGT $n = 1$, CYP3A $n = 16$, CYP2D6 $n = 5$, CYP2C $n = 2$, CYP1A $n = 2$, and Other $n = 2$.

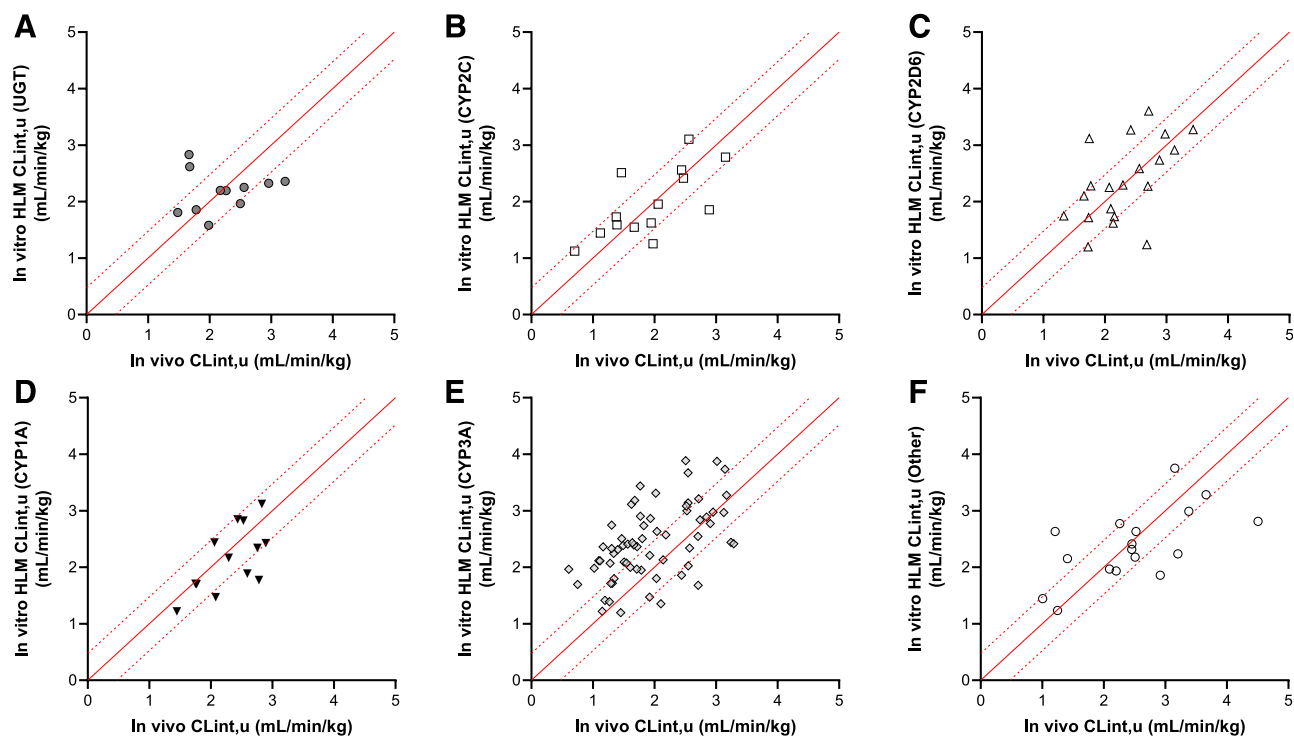


Fig. 4. IVIVE with a regression offset using HLM for substrates of drug metabolism enzyme families. (A) UGT, (B) CYP2C, (C) CYP2D6, (D) CYP1A, (E) CYP3A, and (F) Other. Where, the red solid line is the line of unity, and the red dotted lines represent a 3-fold difference.

Furthermore, based on the data obtained herein, it is reassuring that our current approach of employing an IVIVE regression offset from data generated using HH remains a useful and applicable strategy for all compounds, irrespective of metabolism enzyme. However, in the

authors' opinion, uncertainty in CLmet prediction would increase for compounds that were relatively unstable in HLM compared with a more favorable HH CLint value, which highlights the need to use both HLM and HH CLint data to optimize against in drug discovery.

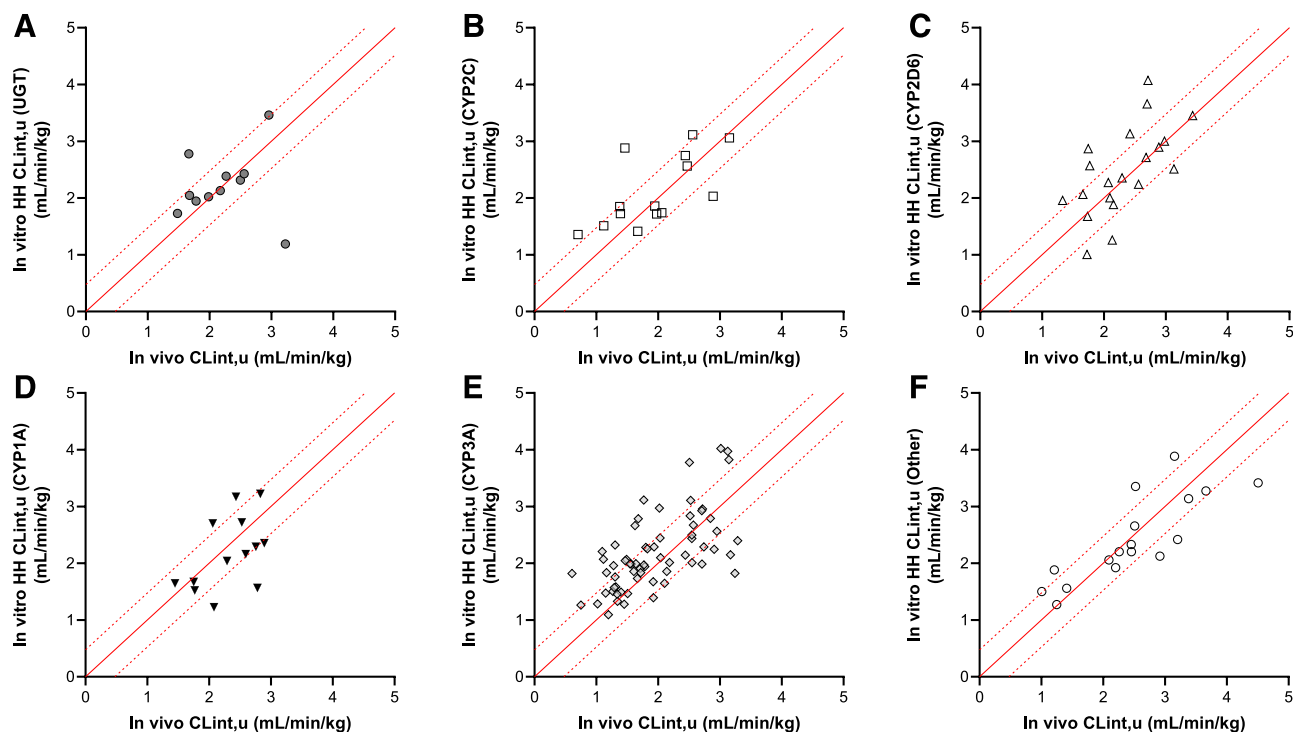


Fig. 5. IVIVE with a regression offset using HH for substrates of drug metabolism enzyme families. (A) UGT, (B) CYP2C, (C) CYP2D6, (D) CYP1A, (E) CYP3A, and (F) Other. Where, the red solid line is the line of unity, and the red dotted lines represent a 3-fold difference.

TABLE 2
IVIVE prediction accuracy with and without a regression offset for CYP3A and non-CYP3A substrates

	Substrates	IVIVE Approach	AFE	AAFE	IVIVE Prediction (%)		
					Over	Correct	Under
HLM	CYP3A	Offset	3.1	4.8	56	33	11
		No Offset	1.1	3.2	20	61	19
	Non-CYP3A	Offset	0.9	2.8	16	68	16
		No Offset	0.3	4.4	4	34	62
HH	CYP3A	Offset	1.6	3.1	27	62	11
		No Offset	0.5	3.2	13	54	33
	Non-CYP3A	Offset	1.1	2.8	22	64	14
		No Offset	0.4	3.8	7	48	45

Underprediction of CL could have detrimental effects on the candidate drug progression and may even result in the termination of the clinical program because of insufficient exposure to test the clinical hypothesis. Hence, in drug discovery, it remains an appropriate if risk-averse strategy to focus on lowering HLM in addition to HH CLint to maximize intrinsic metabolic stability. Thus the authors’ recommendation remains to progress candidate drugs into the clinic with a suitable HH derived CLmet prediction and a correspondingly low HLM CLint. In addition, because a different IVIVE regression offset is now emerging for CYP3A substrates using HLM, the relationship may begin to elucidate a more comprehensive mechanistic understanding of IVIVE rather than the current empirical approach, which, although it is broadly successful, can be improved upon.

In summary, this work highlights the correlation between CYP3A substrates and the HLM:HH disconnect and the subsequent deleterious effect on the accuracy of metabolic CL predictions using HLM with our current IVIVE approach for this group of compounds. We demonstrated the HLM:HH CLint ratio is not correlated with MW, LogD, pKa, human CL, or human Vd. However, more work is required to understand the association, if any, of efflux transporter activity with the HLM:HH disconnect. This work suggests a consistent IVIVE approach can be successfully applied to all compounds using HH irrespective of the main contributing metabolic enzyme and provides enhanced scaling methodologies using HLM. However, without a full mechanistic understanding of this HLM:HH disconnect phenomena, it remains our strategy to minimize both HLM as well as HH CLint.

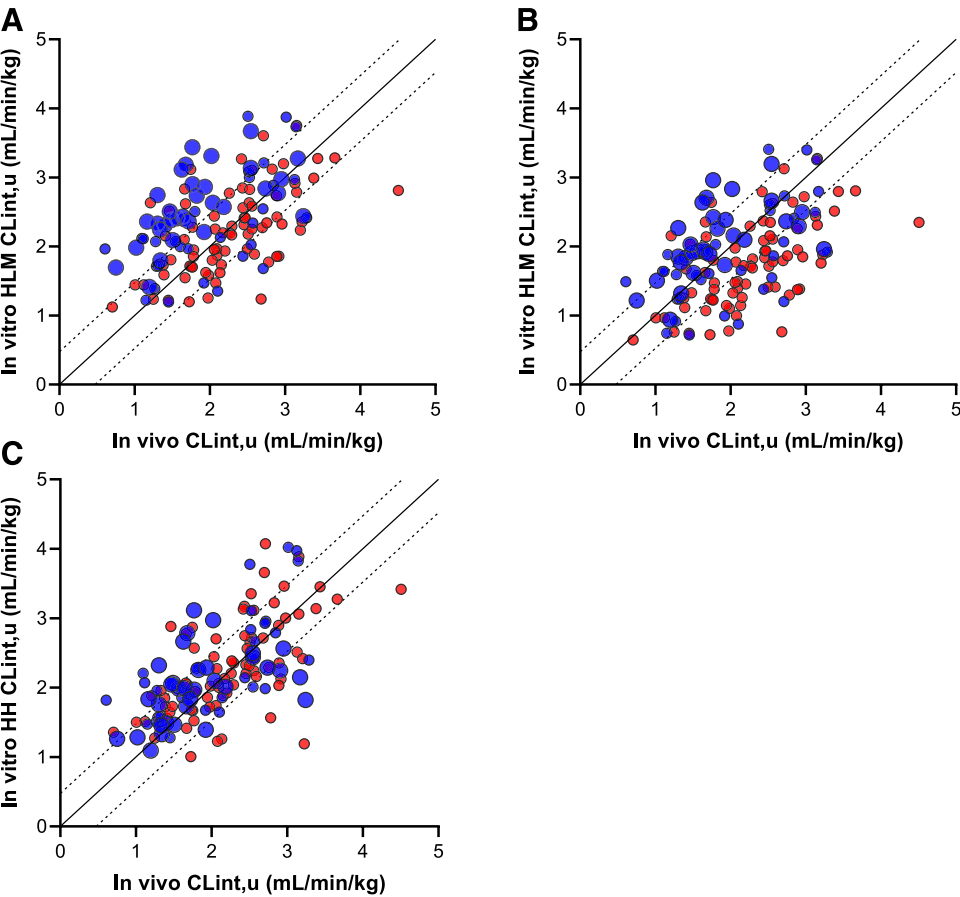


Fig. 6. IVIVE from HLM and HH. Prediction of *in vivo* CLint,u (A) using HLM with a regression offset, (B) using HLM without a regression offset, and (C) using HH with a regression offset. Where, the blue circles represent CYP3A substrates, large blue circles represent CYP3A substrates with an HLM:HH CLint ratio >2, and the red circles represent non-CYP3A substrates. The black solid line is the line of unity, and the black dotted lines represent a 3-fold difference.

Acknowledgments

The authors would like to acknowledge Barry Jones, Tashinga Bapiro, Simone Stahl, Michael Davies, and Jolyon Faria for insightful scientific discussion throughout this work.

Authorship Contributions

Participated in research design: Williamson, Harlfinger, McGinnity.

Conducted experiments: Williamson.

Performed data analysis: Williamson.

Wrote or contributed to the writing of the manuscript: Williamson, Harlfinger, McGinnity.

References

- Berezhkovskiy LM (2011) The corrected traditional equations for calculation of hepatic clearance that account for the difference in drug ionization in extracellular and intracellular tissue water and the corresponding corrected PBPK equation. *J Pharm Sci* **100**:1167–1183.
- Bowman CM and Benet LZ (2016) Hepatic clearance predictions from in vitro-in vivo extrapolation and the biopharmaceutics drug disposition classification system. *Drug Metab Dispos* **44**:1731–1735.
- Bowman CM and Benet LZ (2019a) In vitro-in vivo extrapolation and hepatic clearance-dependent underprediction. *J Pharm Sci* **108**:2500–2504.
- Bowman CM and Benet LZ (2019b) In vitro-in vivo inaccuracy: the CYP3A4 anomaly. *Drug Metab Dispos* **47**:1368–1371.
- Cerny MA (2016) Prevalence of non-cytochrome P450-mediated metabolism in Food and Drug Administration-approved oral and intravenous drugs: 2006–2015. *Drug Metab Dispos* **44**:1246–1252.
- Chen S, Prieto Garcia L, Bergström F, Nordell P, and Grime K (2017) Intrinsic clearance assay incubational binding: a method comparison. *Drug Metab Dispos* **45**:342–345.
- Chiba M, Ishii Y, and Sugiyama Y (2009) Prediction of hepatic clearance in human from in vitro data for successful drug development. *AAPS J* **11**:262–276.
- Davies M, Jones RDO, Grime K, Jansson-Löfmark R, Fretland AJ, Winiwarter S, Morgan P, and McGinnity DF (2020) Improving the accuracy of predicted human pharmacokinetics: lessons learned from the AstraZeneca drug pipeline over two decades. *Trends Pharmacol Sci* **41**:390–408.
- Di L, Keefer C, Scott DO, Strelevitz TJ, Chang G, Bi YA, Lai Y, Duckworth J, Fenner K, Troutman MD, et al. (2012) Mechanistic insights from comparing intrinsic clearance values between human liver microsomes and hepatocytes to guide drug design. *Eur J Med Chem* **57**:441–448, doi: 10.1016/j.ejmech.2012.06.043 In press.
- Dinno A (2015) Nonparametric pairwise multiple comparisons in independent groups using Dunn's test. *Stata J* **15**:292–300.
- Foster JA, Houston JB, and Hallifax D (2011) Comparison of intrinsic clearances in human liver microsomes and suspended hepatocytes from the same donor livers: clearance-dependent relationship and implications for prediction of in vivo clearance. *Xenobiotica* **41**:124–136.
- Hay M, Thomas DW, Craighead JL, Economides C, and Rosenthal J (2014) Clinical development success rates for investigational drugs. *Nat Biotechnol* **32**:40–51.
- Huang L, Berry L, Ganga S, Janosky B, Chen A, Roberts J, Colletti AE, and Lin MH (2010) Relationship between passive permeability, efflux, and predictability of clearance from in vitro metabolic intrinsic clearance. *Drug Metab Dispos* **38**:223–231.
- Kim RB, Wandel C, Leake B, Cvetkovic M, Fromm MF, Dempsey PJ, Roden MM, Belas F, Chaudhary AK, Roden DM, et al. (1999) Interrelationship between substrates and inhibitors of human CYP3A and P-glycoprotein. *Pharm Res* **16**:408–414.
- Lombardo F, Berellini G, and Obach RS (2018) Trend analysis of a database of intravenous pharmacokinetic parameters in humans for 1352 drug compounds. *Drug Metab Dispos* **46**:1466–1477.
- McDonald JH (2014a) *Handbook of Biological Statistics*, 3rd ed pp 157–164, Sparky House Publishing, Baltimore, MD.
- McDonald JH (2014b) *Handbook of Biological Statistics*, 3rd ed pp 186–189, Sparky House Publishing, Baltimore, MD.
- Riley RJ, McGinnity DF, and Austin RP (2005) A unified model for predicting human hepatic, metabolic clearance from in vitro intrinsic clearance data in hepatocytes and microsomes. *Drug Metab Dispos* **33**:1304–1311.
- Rowland M, Benet LZ, and Graham GG (1973) Clearance concepts in pharmacokinetics. *J Pharmacokinet Biopharm* **1**:123–136.
- Shebley M, Liu J, Kavetskaia O, Sydor J, de Morais SM, Fischer V, Nijssen MJMA, and Bow DAJ (2017) Mechanisms and predictions of drug-drug interactions of the hepatitis C virus three direct-acting antiviral regimen: paritaprevir/ritonavir, ombitasvir, and dasabuvir. *Drug Metab Dispos* **45**:755–764.
- Sohlenius-Sternbeck AK, Jones C, Ferguson D, Middleton BJ, Projean D, Floby E, Bylund J, and Afzelius L (2012) Practical use of the regression offset approach for the prediction of in vivo intrinsic clearance from hepatocytes. *Xenobiotica* **42**:841–853.
- Stringer R, Nicklin PL, and Houston JB (2008) Reliability of human cryopreserved hepatocytes and liver microsomes as in vitro systems to predict metabolic clearance. *Xenobiotica* **38**:1313–1329.
- Weaver KF, Morales VC, Dunn SL, Godde K, and Weaver PF (2017) Kruskal-Wallis, *An Introduction to Statistical Analysis in Research* pp 353–391, John Wiley & Sons Inc., Hoboken, NJ.
- Williamson B, Colclough N, Fretland AJ, Jones BC, Jones RDO, and McGinnity DF (2020) Further considerations towards an effective and efficient oncology drug discovery DMPK strategy. *Curr Drug Metab* **21**:145–162.
- Winiwarter S, Chang G, Desai P, Menzel K, Faller B, Arimoto R, Keefer C, and Broccatelli F (2019) Prediction of fraction unbound in microsomal and hepatocyte incubations: a comparison of methods across industry datasets. *Mol Pharm* **16**:4077–4085.
- Wood FL, Houston JB, and Hallifax D (2017) Clearance prediction methodology needs fundamental improvement: trends common to rat and human hepatocytes/microsomes and implications for experimental methodology. *Drug Metab Dispos* **45**:1178–1188.
- Yang J, Jamei M, Yeo KR, Rostami-Hodjegan A, and Tucker GT (2007) Misuse of the well-stirred model of hepatic drug clearance. *Drug Metab Dispos* **35**:501–502.

Address correspondence to: Beth Williamson, AstraZeneca, Hodgkin Bldg., c/o Darwin Bldg., Unit 310, Cambridge Science Park, Milton Rd., Cambridge CB4 0WG, UK. E-mail: beth.williamson1@astrazeneca.com

Evaluation of the disconnect between hepatocyte and microsome intrinsic clearance and in vitro in vivo extrapolation performance.

Beth Williamson, Stephanie Harlfinger, Dermot F McGinnity

Drug Metabolism and Pharmacokinetics, Research and Early Development, Oncology R&D, AstraZeneca, Cambridge, UK.

Table S1. Compound physicochemical properties and *in vitro* ADME data.

Name	MW	Ion Class	HBD	HBA	TPSA	ACD pKa A ₁	ACD pKa B ₁	LogD	ACD LogP	Human Hep CLint ($\mu\text{L}/\text{min}/\times 10^6$)	Human Mic CLint ($\mu\text{L}/\text{min}/\text{mg}$)	fu _{inc}	Human fu _p	Main isoform
Chlorpromazine	318.9	Base		2	32		9.6	3.4	5.4	20	39	0.060	0.026	CYP2D6
Prochlorperazine	374.0	Base		3	35		7.7	3.6	4.8	12	2	0.023	0.141	CYP2D6
Dipyridamole	504.6	Neutral	4	12	145		6.5	3.8	0.3	28	96	0.407	0.048	UGT
Erlotinib	393.4	Neutral	1	7	75		5.5	3.3	3.0	5	20	0.504	0.052	CYP3A
Promethazine	284.4	Base		2	32		9.1	2.8	4.6	9	1	0.144	0.090	CYP2D6
Propranolol	259.4	Base	2	3	41		9.5	1.3	3.3	10	29	0.467	0.243	CYP2D6
Rosiglitazone	357.4	Neutral	1	5	97	6.3	6.5	2.5	2.8	13	37	0.514	0.003	Other
Ondansetron	293.4	Base		4	40		6.8	1.6	2.8	3	8	0.842	0.435	CYP3A
Amsacrine	393.5	Neutral	2	5	89	8.2		3.1	3.2	11	40	0.434	0.007	CYP1A
Antazoline	265.4	Base	1	3	28		10.3	1.4	3.6	52	195	0.726	0.562	CYP3A
Gefitinib	446.9	Base	1	7	69		7.0	3.7	3.7	4	44	0.214	0.035	CYP3A
Edaravone	174.2	Neutral	1	3	33		2.7	0.5	1.1	2	65	0.828	0.001	UGT
Semaxanib	238.3	Neutral	2	2	45	13.2	1.5	3.4	3.0	28	68	0.036	0.031	CYP3A
Verapamil	454.6	Base		6	64		8.1	2.6	4.0	23	180	0.548	0.155	CYP3A
Imatinib	493.6	Base	2	7	86	13.3	7.6	2.5	3.1	3	35	0.405	0.085	CYP3A
Cyclizine	266.4	Base		2	6		7.5	2.4	2.8	5	10	0.515	0.339	CYP2D6
Promazine	284.4	Base		2	32		9.6	2.5	4.7	26	37	0.151	0.158	CYP1A

Diazepam	284.8	Neutral		2	33		3.4	2.7	2.9	5	11	0.566	0.016	CYP2C
Melatonin	232.3	Neutral	2	3	54			1.3	1.7	2	10	0.931	0.679	CYP1A
Trazodone	371.9	Base		6	42		7.5	2.6	2.8	7	26	0.645	0.079	CYP3A
Papaverine	339.4	Neutral		5	50		6.3	2.8	3.2	35	48	0.636	0.063	CYP3A
Trimipramine	294.4	Base		2	6		9.6	3.0	5.0	14	29	0.153	0.091	CYP2D6
Alprenolol	249.4	Base	2	3	41		9.4	1.0	2.8	17	110	0.826	0.150	CYP2D6
Ketamine	237.7	Base	1	2	29		7.7	1.7	2.1	11	36	0.970	0.652	CYP3A
Fluphenazine	437.5	Base	1	4	55		7.4	3.8	4.5	46	47	0.034	0.035	CYP2D6
Clomipramine	314.9	Base		2	6		9.7	3.3	5.3	9	27	0.061	0.037	CYP2C
Voriconazole	349.3	Neutral	1	6	77	11.3	3.1	1.7	1.4	5	12	0.860	0.566	CYP2C
Benperidol	381.5	Base	1	5	53	12.0	8.9	2.7	4.0	10	49	0.441	0.219	CYP3A
Warfarin	308.3	Neutral	1	4	64		4.9	0.9	3.1	3	4	1.018	0.011	CYP2C
Bevantolol	345.4	Base	2	5	60		8.9	1.7	2.7	22	33	0.508	0.127	CYP2D6
Diltiazem	414.5	Base		4	84		9.1	2.0	3.4	7	39	0.834	0.265	CYP3A
Bupivacaine	288.4	Base	1	2	32		8.1	2.5	3.1	9	73	0.816	0.148	CYP3A
Riluzole	234.2	Neutral	2	3	76		3.0	3.3	2.4	10	35	0.459	0.043	CYP1A
Citalopram	324.4	Base		3	36		9.8	1.5	3.4	2	5	0.556	0.411	CYP2C
Prazosin	383.4	Neutral	2	8	107		6.5	1.9	1.2	4	7	0.853	0.048	CYP3A
Mebendazole	295.3	Neutral	2	4	84	7.4	4.8	2.9	2.8	10	16	0.632	0.066	Other
Biperiden	311.5	Base	1	2	23		9.3	2.5	4.2	7	35	0.388	0.100	Unknown
Adinazolam	351.8	Base		5	46		6.9	1.4	2.3	3	55	0.780	0.352	CYP3A
Tolfenamic Acid	261.7	Acid	1	3	49	3.7		1.4	5.5	128	28	0.381	0.003	UGT
Tolamolol	344.4	Base	4	5	94		8.1	1.5	1.7	8	19	0.712	0.348	CYP2D6
Chlorambucil	304.2	Acid		3	41	4.8	4.6	1.5	3.1	44	44	0.809*	0.010	Other

Risperidone	410.5	Base		6	62		8.1	2.1	2.6	9	31	0.706	0.160	CYP2D6
Ziprasidone	412.9	Base	1	4	77	13.3	6.8	2.5	4.1	15	45	0.067	0.001	Other
Flavopiridol	401.8	Base	3	6	90		9.3	1.7	2.8	9	9	0.702	0.090	UGT
Metopimazine	445.6	Base	2	5	117		8.4	1.1	3.1	33	22	1.011	0.273	Other
Midazolam	325.8	Neutral		3	30		6.3	3.4	3.4	19	295	0.617	0.020	CYP3A
Nefopam	253.3	Base		2	12		9.2	2.2	3.5	4	14	0.803	0.507	CYP1A
Tolterodine	325.5	Base	1	2	23	10.2	10.1	1.8	5.4	30	160	0.352	0.253	CYP2D6
Azelastine	381.9	Base		4	36		9.4	2.4	4.3	3	31	0.205	0.145	CYP3A
Enoximone	248.3	Neutral	2	4	84	10.4		1.1	2.1	4	19	0.919	0.410	CYP1A
Propafenone	341.5	Base	2	4	59		9.3	1.7	3.4	31	148	0.269	0.074	CYP2D6
Dofetilide	441.6	Base	2	6	122	9.1	8.3	0.6	1.7	3	4	0.891	0.490	CYP3A
Procyclidine	287.4	Base	1	2	23		10.1	1.8	4.0	4	18	0.552	0.222	CYP3A
Mibefradil	495.6	Base	1	5	67	11.9	9.4	3.5	6.1	26	57	0.022	0.005	CYP3A
Domperidone	425.9	Base	2	7	68	11.1	9.0	3.4	4.2	17	90	0.158	0.034	CYP3A
Carvedilol	406.5	Base	3	6	76		8.2	3.3	4.1	27	64	0.140	0.019	CYP1A
Pantoprazole	383.4	Neutral	1	7	106		3.8	2.0	1.5	8	13	0.922	0.028	CYP2C
Ropivacaine	274.4	Base	1	2	32		8.1	2.1	2.7	10	65	0.776	0.242	CYP3A
Mirtazapine	265.4	Base		3	19		8.1	2.8	3.0	4	13	0.690	0.239	CYP2D6
Zolpidem	307.4	Neutral		3	38	13.4	6.7	2.4	3.1	5	9	0.869	0.065	CYP3A
Mepivacaine	246.4	Base	1	2	32		8.3	1.5	1.9	1	9	0.958	0.524	CYP3A
Venlafaxine	277.4	Base	1	3	33		9.4	0.9	3.2	1	5	0.927	0.827	CYP2D6
Verlukaast	515.1	Acid		4	121		3.6	2.9	5.4	11	43	0.183	0.002	CYP1A
Doxazosin	451.5	Neutral	2	9	112		6.5	2.5	1.5	4	38	0.345	0.059	CYP3A
Ranolazine	427.5	Base	2	6	74		6.5	2.6	2.5	6	24	0.699	0.435	CYP3A

Pimobendan	334.4	Neutral	2	5	79	4.5		1.1	1.8	9	14	0.519	0.110	CYP1A
Dexmedetomidine	200.3	Base	1	2	29	13.9	6.6	2.8	2.9	5	14	0.471	0.148	Other
Finasteride	372.6	Neutral	2	2	58			3.3	3.0	2	10	0.562	0.139	CYP3A
Levomepromazine	328.5	Base		3	41		9.5	3.0	4.9	13	31	0.089	0.056	CYP3A
Clarithromycin	748.0	Base	4	13	183		9.2	1.6	3.1	2	25	0.585	0.350	CYP3A
Prednisone	358.4	Neutral	2	5	92			1.3	1.6	17	42	0.933	0.270	CYP3A
Triamcinolone Acetonide	434.5	Neutral	2	6	93			2.3	2.6	9	219	0.790	0.292	CYP3A
Cilomilast	343.4	Acid		5	80	4.3		0.8	3.4	3	11	0.901	0.011	CYP2C
Granisetron	312.4	Base	1	4	50	12.3	9.8	0.7	2.1	5	4	0.970	0.607	CYP1A
Paroxetine	329.4	Base	1	4	40		9.7	1.8	3.7	3	20	0.069	0.102	CYP2D6
Thalidomide	258.2	Neutral	1	4	84	10.7		0.6	0.5	4	11	1.119	0.400	Other
Quinine	324.4	Base	1	4	46	12.9	8.6	2.0	3.0	1	19	0.581	0.199	CYP3A
Levonorgestrel	312.5	Neutral	1	2	37			3.5	3.3	6	47	0.498	0.045	CYP3A
Roflumilast	403.2	Neutral	1	4	60	9.9	0.6	3.6	4.1	3	8	0.301	0.005	CYP3A
Flupentixol	434.5	Base	1	3	52		8.0	4.0	4.6	12	45	0.017	0.016	CYP3A
Irinotecan	586.7	Base	1	7	113	10.8	9.5	0.7	3.8	4	16	0.713	0.397	UGT
Clindamycin	425.0	Base	4	6	128		8.7	1.6	2.1	5	55	0.745	0.286	CYP3A
Idrocilamide	191.2	Neutral	2	2	49			1.1*	0.9	51	65	0.578	0.036	CYP2C
Doxepin	279.4	Base		2	12		9.3	2.4	4.3	10	27	0.399	0.221	CYP2D6
Selegiline	187.3	Base		1	3		7.4	2.5	2.9	23	46	0.763	0.369	Other
Nortilidine	259.4	Base	1	2	38		9.1	1.1	2.7	2	20	0.936	0.862	CYP3A
Ridogrel	366.3	Acid		5	72	4.7	3.6	1.3	3.6	2	5	0.776	0.063	Unknown
Erythromycin	733.9	Base	5	13	194	13.5	9.2	1.0	2.4	3	52	0.856	0.353	CYP3A

Zimeldine	317.2	Base		2	16		7.9	2.3	3.7	7	18	0.546	0.333	Other
Hydrocortisone	362.5	Neutral	3	5	95			1.5	1.7	10	42	2.342	0.380	CYP3A
Tozasertib	464.6	Base	3	8	127	12.8	7.1	3.4	1.9	29	61	0.181	0.069	Other
Dimetindene maleate	292.4	Base		2	16		9.8	2.1*	3.9	6	11	0.576	0.294	CYP2D6
Axitinib	386.5	Neutral	2	4	96	12.2	4.3	3.7	3.7	9	28	0.325*	0.003	CYP3A
Panobinostat	349.4	Base	4	4	77	8.7	9.3	1.1	3.0	5	22	0.513	0.391	CYP3A
1-hydroxymidazolam	341.8	Neutral	1	4	50	14.0	3.9	2.7	2.6	20	38	0.696	0.098	UGT
Nateglinide	317.4	Acid	1	3	66			0.7	4.2	5	27	0.852	0.017	CYP2C
Alfuzosin	389.5	Neutral	3	8	112		8.4	1.2	1.0	2	5	0.947	0.292	CYP3A
Danuserib	474.6	Base	2	7	94	13.4	7.6	2.0	2.6	3	35	0.705	0.337	Other
Repaglinide	452.6	Acid	1	5	79	4.2	5.8	2.2	4.9	35	47	0.223	0.009	CYP2C
Reboxetine	313.4	Base	1	4	40		8.4	1.7	3.1	1	9	0.504	0.152	CYP3A
Duloxetine	297.4	Base	1	2	50		10.0	2.1	4.0	9	38	0.059	0.055	CYP2D6
Doxapram	378.5	Base		3	33		7.3	2.3	3.3	7	120	0.803	0.440	Unknown
Vinorelbine	778.9	Base	2	9	134		6.9	2.6	4.8	3	126	0.193	0.400	CYP3A
Gestodene	310.4	Neutral	1	2	37			3.1*	3.1	4	43	0.534	0.057	CYP3A
Encainide	352.5	Base	1	3	42		9.9	2.6*	4.5	9	26	0.858	0.572	CYP2D6
Mizolastine	432.5	Neutral	1	7	66	9.7	7.7	3.0	2.8	6	70	0.486	0.023	UGT
Ramelteon	259.4	Neutral	1	2	38			2.6	3.1	12	48	0.937	0.183	CYP1A
Bortezomib	384.2	Neutral	4	6	124	9.7	0.3	2.1*	1.9	6	73	0.764	0.132	CYP3A
Telcagepant	566.5	Neutral	2	6	98	7.3	5.5	3.3	2.7	4	42	0.323	0.053	CYP3A
AFN-1252	375.4	Neutral	1	4	75	10.3	3.5	2.4	3.0	9	73	0.376	0.047	CYP3A
Olodaterol	386.5	Base	4	6	100	9.4	9.1	0.8	1.8	6	14	0.561	0.516	UGT
Bendamustine	358.3	Acid		5	58	4.5	9.3	1.0	2.9	51	83	0.843*	0.050	CYP1A

Aplaviroc	549.1	Neutral	3	7	159	7.0		2.1	4.2	40	50	0.41*	0.013	CYP3A
Ulimorelin	538.7	Base	3	5	100		7.3	3.3	2.6	35	266	0.503	0.002	CYP3A
Deferasirox	373.4	Acid	2	7	108	3.5	2.2	1.5*	4.3	7	24	0.443	0.006	UGT
Conivaptan	498.6	Neutral	2	4	78	12.8	7.2	3.5*	4.6	5	203	0.124	0.010	CYP3A
Solifenacin	378.5	Base		2	33		8.8	2.4	4.7	4	12	0.269	0.179	CYP3A
Nebivolol	405.4	Base	3	5	71		8.6	3.0	3.7	25	55	0.028	0.030	CYP2D6
Lesinurad	404.3	Acid		5	93	2.9		-0.02	4.6	4	4	0.664	0.016	CYP2C
Dinaciclib	396.5	Cationic	2	7	71		6.7	1.9	1.1	38	323	0.716	0.142	CYP3A
Nintedanib	539.6	Base	2	6	94	11.1	7.4	3.0	2.8	62	46	0.197*	0.016	Other
CUDC-101	434.5	Neutral	3	7	106	9.5	5.8	3.4	3.1	222	66	0.205	0.021	CYP3A
Dabrafenib	519.6	Acid	3	6	147	6.6	2.2	2.9	3.8	15	32	0.351	0.011	CYP2C
Tolvaptan	449.0	Neutral	2	3	70			3.7	4.2	22	145	0.204	0.026	CYP3A
Laropiprant	435.9	Acid		5	85			1.4*	4.5	13	26	0.412	0.004	UGT
Etonogestrel	324.5	Neutral	1	2	37			3.7	3.4	9	84	0.445	0.033	CYP3A
Mirabegron	396.5	Base	5	5	129	13.5	8.9	0.6	2.0	2	11	0.772	0.290	CYP2D6
Gisadenafil	519.6	Base	1	11	140	8.1	6.9	2.1	1.1	2	40	0.718	0.552	CYP3A
Basimglurant	325.8	Neutral		3	31		4.8	4.3	3.8	11	57	0.135	0.010	CYP3A
Canagliflozin	444.5	Neutral	4	5	118			3.0	3.7	6	8	0.297*	0.010	UGT
Fimasartan	501.7	Acid	1	8	122	4.2	1.5	0.6	3.5	5	11	0.441*	0.023	CYP2C
Bunazosin	373.5	Neutral	2	7	94		7.8	1.6*	1.6	6	65	0.804	0.120	CYP3A
Dexloxiglumide	461.4	Acid	1	5	96	4.5		1.4	4.3	11	18	0.712	0.016	CYP3A
Tasimelteon	245.3	Neutral	1	2	38			2.2	2.2	4	17	0.975	0.274	CYP1A
Vilazodone	441.5	Base	3	6	102		7.9	3.4	3.8	3	37	0.145	0.054	CYP3A
Paritaprevir	765.9	Acid	3	10	198	4.4		2.5	2.3	6	69	0.287	0.014	CYP3A

Propiverine	367.5	Base		3	39		7.8	3.4	5.4	28	177	0.186	0.058	CYP3A
Indisulam	385.9	Neutral	4	5	139	8.1		2.1	2.0	12	24	0.187	0.003	CYP2C
Volasertib	618.8	Base	2	9	106		8.0	3.5	3.3	5	54	0.263	0.145	Unknown
Remimazolam	439.3	Neutral		5	69		5.8	5.1	3.1	158	90	0.607*	0.164	Other

Name	Isoform reference
Chlorpromazine	Suzuki Y, Someya T, Shimoda K, Hirokane G, Morita S, Yokono A, Inoue Y, Takahashi S. (2001) Importance of the cytochrome P450 2D6 genotype for the drug metabolic interaction between chlorpromazine and haloperidol. <i>Ther Drug Monit.</i> 23(4): 363-8.
Prochlorperazine	DIDB drug monograph
Dipyridamole	Zhang ZY, Chen M, Chen J, Padval MV and Kansra VV (2009) Biotransformation and in vitro assessment of metabolism-associated drug-drug interaction for CRx-102, a novel combination drug candidate. <i>J Pharm Biomed Anal</i> 50(2): 200-209.
Erlotinib	Li J, Zhao M, He P, Hidalgo M and Baker SD (2007) Differential metabolism of gefitinib and erlotinib by human cytochrome P450 enzymes. <i>Clin Cancer Res</i> 13(12): 3731-3737.
Promethazine	DIDB drug monograph
Propranolol	Bowman CM and Benet LZ (2019) In Vitro–In Vivo Inaccuracy: The CYP3A4 Anomaly. <i>Drug Metab and Dispos</i> 47(12): 1368-1371.
Rosiglitazone	DIDB drug monograph
Ondansetron	Bowman CM and Benet LZ (2019) In Vitro–In Vivo Inaccuracy: The CYP3A4 Anomaly. <i>Drug Metab and Dispos</i> 47(12): 1368-1371.
Amsacrine	Measured in-house
Antazoline	Satoskar RS, Bhandarkar SD and Rege NN (1973) <i>Pharmacology and Pharmacotherapeutics, Volume 1</i> , 21st ed, Popular Prakashan
Gefitinib	Li J, Zhao M, He P, Hidalgo M and Baker SD (2007) Differential metabolism of gefitinib and erlotinib by human cytochrome P450 enzymes. <i>Clin Cancer Res</i> 13(12): 3731-3737.
Edaravone	DIDB drug monograph
Semaxanib	Kieran MW, Supko JG, Wallace D, Fruscio R, Poussaint TY, Phillips P, Pollack I, Packer R, Boyett JM, Blaney S, Banerjee A, Geyer R, Friedman H, Goldman S, Kun LE and Macdonald T; Pediatric Brain Tumor Consortium (2009) Phase I study of SU5416, a small molecule inhibitor of the vascular endothelial growth factor receptor (VEGFR) in refractory pediatric central nervous system tumors. <i>Pediatr Blood Cancer</i> 52(2): 169-176.

Verapamil	Bowman CM and Benet LZ (2019) In Vitro–In Vivo Inaccuracy: The CYP3A4 Anomaly. <i>Drug Metab and Dispos</i> 47(12): 1368-1371.
Imatinib	DIDB drug monograph
Cyclizine	Vella-Brincat JW, Begg EJ, Jensen BP, Chin PK, Roberts RL, Fairhall M, Macleod SA and Reid K (2012) The pharmacokinetics and pharmacogenetics of the antiemetic cyclizine in palliative care patients. <i>J Pain Symptom Manage</i> 43(3): 540-548.
Promazine	Wójcikowski J, Pichard-Garcia L, Maurel P and Daniel WA (2003) Contribution of human cytochrome p-450 isoforms to the metabolism of the simplest phenothiazine neuroleptic promazine. <i>Br J Pharmacol</i> 138(8): 1465-1474.
Diazepam	DIDB drug monograph
Melatonin	Ma X, Idle JR, Krausz KW and Gonzalez FJ (2005) Metabolism of melatonin by human cytochromes p450. <i>Drug Metab Dispos</i> 33(4): 489-494.
Trazodone	Bowman CM and Benet LZ (2019) In Vitro–In Vivo Inaccuracy: The CYP3A4 Anomaly. <i>Drug Metab and Dispos</i> 47(12): 1368-1371.
Papaverine	Measured in-house
Trimipramine	Kirchheiner J, Müller G, Meineke I, Wernecke KD, Roots I and Brockmüller J (2003) Effects of polymorphisms in CYP2D6, CYP2C9, and CYP2C19 on trimipramine pharmacokinetics. <i>J Clin Psychopharmacol</i> 23(5): 459-466.
Alprenolol	Zisaki A, Miskovic L and Hatzimanikatis V (2015) Antihypertensive drugs metabolism: an update to pharmacokinetic profiles and computational approaches. <i>Curr Pharm Des</i> 21(6): 806-822.
Ketamine	Dinis-Oliveira RJ (2017) Metabolism and metabolomics of ketamine: a toxicological approach. <i>Forensic Sci Res</i> 2(1): 2-10.
Fluphenazine	Siragusa S and Saadabadi A (2018) "Fluphenazine" in StatPearls. StatPearls Publishing, Treasure Island FL, USA https://www.ncbi.nlm.nih.gov/books/NBK459194/
Clomipramine	DIDB drug monograph
Voriconazole	DIDB drug monograph
Benperidol	Sun H and Scott DO (2011) Metabolism of 4-Aminopiperidine Drugs by Cytochrome P450s: Molecular and Quantum Mechanical Insights into Drug Design. <i>ACS Med Chem Lett</i> 2(8): 638-643.
Warfarin	Bowman CM and Benet LZ (2019) In Vitro–In Vivo Inaccuracy: The CYP3A4 Anomaly. <i>Drug Metab and Dispos</i> 47(12): 1368-1371.
Bevantolol	Bijl MJ, Visser LE, van Schaik RH, Kors JA, Witteman JC, Hofman A, Vulto AG, van Gelder T and Stricker BH (2009) Genetic variation in the CYP2D6 gene is associated with a lower heart rate and blood pressure in beta-blocker users. <i>Clin Pharmacol Ther</i> 85(1): 45-50.
Diltiazem	Bowman CM and Benet LZ (2019) In Vitro–In Vivo Inaccuracy: The CYP3A4 Anomaly. <i>Drug Metab and Dispos</i> 47(12): 1368-1371.
Bupivacaine	Gantenbein M, Attolini L, Bruguerolle B, Villard PH, Puyoo F, Durand A, Lacarelle B, Hardwigsen J and Le-Treut YP (2000) Oxidative metabolism of bupivacaine into pitecolylxylidine in humans is mainly catalyzed by CYP3A. <i>Drug Metab Dispos</i> 28(4): 383-385.

Riluzole	van Kan HJ, van den Berg LH, Groeneveld GJ, van der Straaten RJ, van Vught PW, Lie-A-Huen L and Guchelaar HJ (2008) Pharmacokinetics of riluzole: evidence for glucuronidation as a major metabolic pathway not associated with UGT1A1 genotype. <i>Biopharm Drug Dispos</i> 29(3): 139-144.
Citalopram	DIDB drug monograph
Prazosin	Measured in-house
Mebendazole	Dayan AD (2003) Albendazole, mebendazole and praziquantel. Review of non-clinical toxicity and pharmacokinetics. <i>Acta Trop</i> 86(2-3): 141-159.
Biperiden	National Center for Biotechnology Information. PubChem Database. Biperiden, CID=2381, https://pubchem.ncbi.nlm.nih.gov/compound/Biperiden (accessed on March, 2020)
Adinazolam	Venkatakrishnan K, von Moltke LL, Duan SX, Fleishaker JC, Shader RI, Greenblatt DJ (1998) Kinetic characterization and identification of the enzymes responsible for the hepatic biotransformation of adinazolam and N-desmethylnadinazolam in man. <i>J Pharm Pharmacol</i> 50(3):265-74.
Tolfenamic Acid	Nakamori F, Naritomi Y, Hosoya K, Moriguchi H, Tetsuka K, Furukawa T, Kadono K, Yamano K, Terashita S and Teramura T (2012) Quantitative prediction of human intestinal glucuronidation effects on intestinal availability of UDP-glucuronosyltransferase substrates using in vitro data. <i>Drug Metab Dispos</i> 40(9): 1771-1777.
Tolamolol	Measured in-house
Chlorambucil	DIDB drug monograph
Risperidone	DIDB drug monograph
Ziprasidone	DIDB drug monograph
Flavopiridol	Ramírez J, Iyer L, Journault K, Bélanger P, Innocenti F, Ratain MJ and Guillemette C (2002) In vitro characterization of hepatic flavopiridol metabolism using human liver microsomes and recombinant UGT enzymes. <i>Pharm Res</i> 19(5): 588-594.
Metopimazine	Mallet E, Bounoure F, Skiba M, Saussereau E, Goullé JP and Castanet M (2015) Pharmacokinetic study of metopimazine by oral route in children. <i>Pharmacol Res Perspect</i> 3(3): e00130.
Midazolam	Bowman CM and Benet LZ (2019) In Vitro–In Vivo Inaccuracy: The CYP3A4 Anomaly. <i>Drug Metab and Dispos</i> 47(12): 1368-1371.
Nefopam	Tiglis M, Neagu TB, Elfara M, Diaconu CC, Bratu OG, Vacaroiu IA, Grintescu IM (2018) Nefopam and its Role in Modulating Acute and Chronic Pain. <i>Revista de Chimie-Bucharest</i> 69(10): 2877-2880.
Tolterodine	DIDB drug monograph
Azelastine	Nakajima M, Nakamura S, Tokudome S, Shimada N, Yamazaki H and Yokoi T (1999) Azelastine N-demethylation by cytochrome P-450 (CYP)3A4, CYP2D6, and CYP1A2 in human liver microsomes: evaluation of approach to predict the contribution of multiple CYPs. <i>Drug Metab Dispos</i> 27(12): 1381-1391.

Enoximone	Measured in-house
Propafenone	Bowman CM and Benet LZ (2019) In Vitro–In Vivo Inaccuracy: The CYP3A4 Anomaly. <i>Drug Metab and Dispos</i> 47(12): 1368-1371.
Dofetilide	Mounsey JP and DiMarco JP (2000) Dofetilide. <i>Circulation</i> 102: 2665–2670
Procyclidine	Measured in-house
Mibefradil	Welker HA (1998) Single- and multiple-dose mibefradil pharmacokinetics in normal and hypertensive subjects. <i>J Pharm Pharmacol</i> 50(9):983-987.
Domperidone	Bowman CM and Benet LZ (2019) In Vitro–In Vivo Inaccuracy: The CYP3A4 Anomaly. <i>Drug Metab and Dispos</i> 47(12): 1368-1371.
Carvedilol	Bowman CM and Benet LZ (2019) In Vitro–In Vivo Inaccuracy: The CYP3A4 Anomaly. <i>Drug Metab and Dispos</i> 47(12): 1368-1371.
Pantoprazole	DIDB drug monograph
Ropivacaine	Oda Y, Furuichi K, Tanaka K, Hiroi T, Imaoka S, Asada A, Fujimori M and Funae Y (1995) Metabolism of a new local anesthetic, ropivacaine, by human hepatic cytochrome P450. <i>Anesthesiology</i> 82(1): 214-220.
Mirtazapine	DIDB drug monograph
Zolpidem	Bowman CM and Benet LZ (2019) In Vitro–In Vivo Inaccuracy: The CYP3A4 Anomaly. <i>Drug Metab and Dispos</i> 47(12): 1368-1371.
Mepivacaine	Measured in-house
Venlafaxine	DIDB drug monograph
Verlukast	Grossman SJ, Herold EG, Drey JM, Alberts DW, Umbenhauer DR, Patrick DH, Nicoll-Griffith D, Chauret N and Yergey JA (1993) CYP1A1 specificity of Verlukast epoxidation in mice, rats, rhesus monkeys, and humans. <i>Drug Metab Dispos</i> 21(6): 1029-1036.
Doxazosin	https://www.accessdata.fda.gov/drugsatfda_docs/label/2010/021269s011lbl.pdf
Ranolazine	Trujillo TC (2006) Advances in the management of stable angina. <i>J Manag Care Pharm</i> 12(8 Suppl): S10-16.
Pimobendan	Kuriya S, Ohmori S, Hino M, Ishii I, Nakamura H, Senda C, Igarashi T, Kiuchi M and Kitada M (2000) Identification of cytochrome P-450 isoform(s) responsible for the metabolism of pimobendan in human liver microsomes. <i>Drug Metab Dispos</i> 28(1): 73-78.
Dexmedetomidine	Kohli U, Pandharipande P, Muszkat M, Sofowora GG, Friedman EA, Scheinin M, Wood AJ, Ely EW, Tyndale RF, Choi L, Stein CM and Kurnik D (2012) CYP2A6 genetic variation and dexmedetomidine disposition. <i>Eur J Clin Pharmacol</i> 68(6): 937-942.
Finasteride	Hulin-Curtis SL, Petit D, Figg WD, Hsing AW and Reichardt JK (2010) Finasteride metabolism and pharmacogenetics: new approaches to personalized prevention of prostate cancer. <i>Future Oncol</i> 6(12): 1897-1913.
Levomepromazine	Wójcikowski J, Basińska A and Daniel WA (2014) The cytochrome P450-catalyzed metabolism of levomepromazine: a phenothiazine neuroleptic with a wide spectrum of clinical application. <i>Biochem Pharmacol</i> 90(2): 188-195.

Clarithromycin	Lynch T and Price A (2007) The Effect of Cytochrome P450 Metabolism on Drug Response, Interactions, and Adverse Effects. <i>Am Fam Physician</i> 76(3): 391-396.
Prednisone	DIDB drug monograph
Triamcinolone Acetonide	Moore CD, Roberts JK, Orton CR, Murai T, Fidler TP, Reilly CA, Ward RM and Yost GS (2012) Metabolic pathways of inhaled glucocorticoids by the CYP3A enzymes. <i>Drug Metab Dispos</i> 41(2): 379-389.
Cilomilast	Giembycz MA (2006) An update and appraisal of the cilomilast Phase III clinical development programme for chronic obstructive pulmonary disease. <i>Br J Clin Pharmacol</i> 62(2): 138-152.
Granisetron	DIDB drug monograph
Paroxetine	DIDB drug monograph
Thalidomide	Teo SK, Sabourin PJ, O'Brien K, Kook KA and Thomas SD (2000) Metabolism of thalidomide in human microsomes, cloned human cytochrome P-450 isozymes, and Hansen's disease patients. <i>J Biochem Mol Toxicol</i> 14(3): 140-147.
Quinine	https://doi.org/10.3389/fphar.2019.00591
Levonorgestrel	Moreno I, Quiñones L, Catalán J, Miranda C, Roco Á, Sasso J, Tamayo E, Cáceres D, Tchernitchin AN, Gaete L and Saavedra I (2012) Influence of CYP3A4/5 polymorphisms in the pharmacokinetics of levonorgestrel: a pilot study. <i>Biomedica</i> 32(4): 570-577.
Roflumilast	DIDB drug monograph
Flupentixol	Measured in-house
Irinotecan	DIDB drug monograph
Clindamycin	Murphy PB and Le JK (2018) "Clindamycin," in StatPearls. StatPearls Publishing, Treasure Island, FL, USA. https://www.ncbi.nlm.nih.gov/books/NBK519574/
Idrocilamide	Measured in-house
Doxepin	DIDB drug monograph
Selegiline	DIDB drug monograph
Nortilidine	Measured in-house
Ridogrel	Wilson TW and Quest DW (2000) Ridogrel: An Antiplatelet Agent with Antihypertensive Properties. <i>Cardiovas Drug Rev</i> 18(3): 222–231.
Erythromycin	DIDB drug monograph
Zimeldine	Krueger SK, Williams DE (2005) Mammalian flavin-containing monooxygenases: structure/function, genetic polymorphisms and role in drug metabolism. <i>Pharmacol Ther</i> 106(3): 357-387.

Hydrocortisone	Measured in-house
Tozasertib	https://www.ncbi.nlm.nih.gov/pmc/articles/PMC3588010/
Dimetindene maleate	Measured in-house
Axitinib	DIDB drug monograph
Panobinostat	Hamberg P, Woo MM, Chen LC, Verweij J, Porro MG, Zhao L, Li W, van der Biessen D, Sharma S, Hengelage T and de Jonge M (2011) Effect of ketoconazole-mediated CYP3A4 inhibition on clinical pharmacokinetics of panobinostat (LBH589), an orally active histone deacetylase inhibitor. <i>Cancer Chemother Pharmacol</i> 68(3):805-813.
1-hydroxymidazolam	Seo KA, Bae SK, Choi YK, Choi CS, Liu KH and Shin JG (2010) Metabolism of 1'- and 4-hydroxymidazolam by glucuronide conjugation is largely mediated by UDP-glucuronosyltransferases 1A4, 2B4, and 2B7. <i>Drug Metab Dispos</i> 38(11): 2007-2013.
Nateglinide	DIDB drug monograph
Alfuzosin	https://www.accessdata.fda.gov/drugsatfda_docs/label/2008/021287s011lbl.pdf
Danuserib	Catucci G, Occhipinti A, Maffei M, Gilardi G and Sadeghi SJ (2013) Effect of Human Flavin-Containing Monooxygenase 3 Polymorphism on the Metabolism of Aurora Kinase Inhibitors. <i>Int J Mol Sci</i> 14(2): 2707–2716.
Repaglinide	DIDB drug monograph
Reboxetine	Fleishaker JC (2000) Clinical pharmacokinetics of reboxetine, a selective norepinephrine reuptake inhibitor for the treatment of patients with depression. <i>Clin Pharmacokinet</i> 39(6): 413-427.
Duloxetine	DIDB drug monograph
Doxapram	Not available
Vinorelbine	Kajita J, Kuwabara T, Kobayashi H and Kobayashi S (2000) CYP3A4 is mainly responsible for the metabolism of a new vinca alkaloid, vinorelbine, in human liver microsomes. <i>Drug Metab Dispos</i> 28(9): 1121-1127.
Gestodene	Ward S and Back DJ (1993) Metabolism of gestodene in human liver cytosol and microsomes in vitro. <i>J Steroid Biochem Mol Biol</i> 46(2) 235-243.
Encainide	https://www.fda.gov/drugs/drug-interactions-labeling/drug-development-and-drug-interactions-table-substrates-inhibitors-and-inducers
Mizolastine	Li P, Wei MJ, Zhang ZY, Yin SJ, Wang X, Lou YQ, Kang ZS, Lu Y, Wei X, Zhai SD and Zhang GL (2018) Effects of UGT1A1, CYP3A5 and ABCB1 Genetic Variants on Pharmacokinetics of Antihistamine Drug Mizolastine in Chinese Healthy Volunteers. <i>Basic Clin Pharmacol Toxicol</i> doi: 10.1111/bcpt.13028.
Ramelteon	DIDB drug monograph
Bortezomib	https://www.ema.europa.eu/en/documents/scientific-discussion/velcade-epar-scientific-discussion_en.pdf

Telcagepant	Roller S, Cui D, Laspina C, Miller-Stein C, Rowe J, Wong B and Prueksaritanont T (2009) Preclinical pharmacokinetics of MK-0974, an orally active calcitonin-gene related peptide (CGRP)-receptor antagonist, mechanism of dose dependency and species differences. <i>Xenobiotica</i> 39(1): 33-45.
AFN-1252	Measured in-house
Olodaterol	DIDB drug monograph
Bendamustine	DIDB drug monograph
Aplaviroc	Nichols WG, Steel HM, Bonny T, Adkison K, Curtis L, Millard J, Kabeya K and Clumeck N (2008) Hepatotoxicity observed in clinical trials of aplaviroc (GW873140). <i>Antimicrob Agents Chemother</i> 52(3): 858-865.
Ulimorelin	Measured in-house
Deferasirox	Meyboom RHB (2010) Chapter 23 - Metal antagonists in <i>Side Effects of Drugs Annual Vol 32</i> (Aronson JK ed) pp 425-435 Elsevier. https://doi.org/10.1016/S0378-6080(10)32023-X .
Conivaptan	DIDB drug monograph
Solifenacin	DIDB drug monograph
Nebivolol	Briciu C, Neag M, Muntean D, Boscan C, Buzoianu A, Antonescu O, Gheldiu AM, Achim M, Popa A and Vlase L (2015) Phenotypic differences in nebivolol metabolism and bioavailability in healthy volunteers. <i>Clujul Medical</i> . 88(2): 208-213.
Lesinurad	DIDB drug monograph
Dinaciclib	Zhang D, Mita M, Shapiro GI, Poon J, Small K, Tzontcheva A, Kantesaria B, Zhu Y, Bannerji R and Statkevich P (2012) Effect of aprepitant on the pharmacokinetics of the cyclin-dependent kinase inhibitor dinaciclib in patients with advanced malignancies. <i>Cancer Chemother Pharmacol</i> . 70(6): 891-898.
Nintedanib	DIDB drug monograph
CUDC-101	Measured in-house
Dabrafenib	DIDB drug monograph
Tolvaptan	DIDB drug monograph
Laropiprant	Gibson CR, Lu P, Maciolek C, Wudarski C, Barter Z, Rowland-Yeo K, Stroh M, Lai E and Nicoll-Griffith DA (2013) Using human recombinant UDP-glucuronosyltransferase isoforms and a relative activity factor approach to model total body clearance of laropiprant (MK-0524) in humans. <i>Xenobiotica</i> 43(12): 1027-1036.
Etonogestrel	Maddox DD and Rahman Z (2008) Etonogestrel (Implanon), Another Treatment Option for Contraception. <i>Pharmacy and Ther</i> 33(6): 337-347.

Mirabegron	DIDB drug monograph
Gisadenafil	Measured in-house
Basimglurant	Fowler S, Guerini E, Qiu N, Cleary Y, Parrott N, Greig G and Mallalieu NL (2017) Low Potential of Basimglurant to Be Involved in Drug-Drug Interactions: Influence of Non-Michaelis-Menten P450 Kinetics on Fraction Metabolized. <i>J Pharmacol Exp Ther</i> 360: 164–173.
Canagliflozin	DIDB drug monograph
Fimasartan	Choi YJ, Lee JY, Ryu CS, Chi YH, Paik SH and Kim SK (2018) Role of cytochrome P450 enzymes in fimasartan metabolism in vitro. <i>Food Chem Toxicol</i> 115: 375-384.
Bunazosin	Measured in-house
Dexloxiglumide	Persiani S, D'Amato M, Jakate A, Roy P, Wangsa J, Kapil R and Rovati LC (2006) Pharmacokinetic profile of dexloxiglumide. <i>Clin Pharmacokinet</i> 45(12): 1177-1188.
Tasimelteon	DIDB drug monograph
Vilazodone	DIDB drug monograph
Paritaprevir	Shebley M, Liu J, Kavetskaia O, Sydor J, de Moraes SM, Fischer V, Nijsen MJMA and Bow DAJ (2017) Mechanisms and Predictions of Drug-Drug Interactions of the Hepatitis C Virus Three Direct-Acting Antiviral Regimen: Paritaprevir/Ritonavir, Ombitasvir, and Dasabuvir. <i>Drug Metab and Dispos</i> 45(7): 755-764.
Propiverine	DIDB drug monograph
Indisulam	Zandvliet AS, Huitema AD, Copalu W, Yamada Y, Tamura T, Beijnen JH and Schellens JH (2007) CYP2C9 and CYP2C19 polymorphic forms are related to increased indisulam exposure and higher risk of severe hematologic toxicity. <i>Clin Cancer Res</i> 13(10): 2970-2976.
Volasertib	Lin CC, Su WC, Yen CJ, Hsu CH, Su WP, Yeh KH, Lu YS, Cheng AL, Huang DC, Fritsch H, Voss F, Taube T and Yang JC (2014) A phase I study of two dosing schedules of volasertib (BI 6727), an intravenous polo-like kinase inhibitor, in patients with advanced solid malignancies. <i>Br J Cancer</i> 110(10): 2434-2440.
Remimazolam	Goudra BG and Singh PM (2014) Remimazolam: The future of its sedative potential. <i>Saudi J Anaesth</i> . 8(3): 388-91.

Unless noted otherwise, all *in vitro* data was determined in-house and human PK was extracted from Lombardo *et al.*, 2018.

Where possible, the main hepatic metabolic route of elimination was obtained from the literature including the University of Washington Drug Interaction Database (DIDB) (this information is based on or an extract from DIDB Copyright University of Washington, accessed: April 2020).

Where, * represents data generated from in-house machine learning *in silico* models.

The isoform data represents a mixture of clinical or hepatic *in vitro* data. It was assumed the clinical disposition pathway obtained from the literature reflects the main metabolic pathway in HH and HLM.